NPS ARCHIVE
1964
BERTHE, C.

LONGITUDINAL STABILITY OF THE GOODYEAR INFLATOPLANE

by

LCDR. Charles J. Berthe, Jr., USN
LCDR. Peter B. Wyckoff, USN
Lt. John R. Baals, USN

Department of Aerospace and Mechanical Sciences

Report No. 689

DEI SUB NUMINE VIGET

PRINCETON UNIVERSITY

DEPARTMENT OF
AEROSPACE AND MECHANICAL SCIENCES

Thesis
B458

Library
U. S. Naval Postgraduate School
Monterey, California

DUDLEY KNOX LIBRARY
NAVAL POSTGRADUATE SCHOOL
MONTEREY CA 93943-5101

LONGITUDINAL STABILITY OF THE GOODYEAR INFLATOPLANE

by

LCDR. Charles J. Berthe, Jr., USN
LCDR. Peter B. Wyckoff, USN
Lt. John R. Baals, USN

Department of Aerospace and Mechanical Sciences

Report No. 689

Submitted in partial fulfillment of the requirements
for the Degree of Master of Science in Engineering
from Princeton University, June 1964

U. S. Naval Postgraduate School
Monterey, California

ACKNOWLEDGEMENTS

The authors wish to express their appreciation and gratitude to Professor Edward Seckel of the Department of Aerospace and Mechanical Sciences of Princeton University for his guidance and supervision during this investigation.

Most sincere gratitude is extended to the United States Navy for providing the opportunity for postgraduate education.

Appreciation is further extended to Mr. Thomas E. Sweeney and the hangar staff, especially Messrs. W. B. Nixon and S. A. Weissenburger for their assistance in the installation of the required instrumentation and in providing excellent maintenance of the test aircraft.

The authors wish also to thank Mr. Andrew Rostas of the Forrestal Research Center Photo Laboratory for his preparation of illustrations and timely processing of flight test recorder film.

A special thanks also to Mrs. Grace Arnesen who typed the manuscript.

TABLE OF CONTENTS

	Page
LIST OF FIGURES	iii
LIST OF SYMBOLS	v
SUMMARY	1
INTRODUCTION	2
EQUIPMENT	3
ANALYTICAL PROCEDURES	9
FLIGHT TEST PROCEDURES	26
DISCUSSION OF RESULTS	39
CONCLUSIONS	44
REFERENCES	45
TABLES	47
FIGURES	

LIST OF FIGURES

Figure No.

1 Three View Drawing
2 Air Photo of Aircraft
3 Left Side View of Aircraft
4 Right Side View of Aircraft
5 Rear View of Aircraft
6 Exposed View of Air Mat
7 Instrument Panel
8 Recorder and Battery Location
9 Elevator Potentiometer Location
10 Angle of Attack Boom, Camera, and Venturi
11 Instrument Wiring Diagram
12 Instrument Schematic
13 Analog Computer Wiring Diagram
14 Analog Computer Solution, Rigid Aircraft
15 Analog Computer Solutions, Varying $C_{m_{i_t}}$
16 Root Locus for Varying $C_{m_{i_t}}$ and $C_{L_\alpha} = 3.0, 4.0,$ and 5.0 per radian
17 Stable Phugoid Portion of Root Locus
18 Damping Ratio of Oscillatory Transients as a Function of Subsidence Ratio for Second Order Systems
19 Center of Gravity and Gross Weight versus Fuel Quantity and Pilot Weight
20 Wake Survey for Determination of η_t
21 Airspeed Calibration
22 SFIM Recorder Tapes N_o, N_m, Elevator Flutter
23 Flight Test Data, April 5, 1964
24 Flight Test Data, April 10, 1964

LIST OF FIGURES (Continued)

Figure No.

25 Flight Test Data, April 11, 1964

26 Flight Test Data, April 17, 1964

27 Flight Test Data, April 26, 1964

28 Flight Test Data, April 27, 1964

29 Flight Test Data, May 3, 1964

30 Determination of Stick Fixed Neutral Points from Flight Test

31 Determination of Stick Fixed Maneuver Points from Flight Test

32 Composit Neutral and Maneuver Point Curves

33 SFIM Recorder Tape, Phugoid and Noise

34 Selected Prints from Movie Camera Showing Fuselage Bending

35 Determination of $C_{m_{i_t}}$ and τ_e from Flight Test

LIST OF SYMBOLS

Capital Letters

A	Area
AR	Aspect ratio
C_D	Drag coefficient
C_L	Lift coefficient
C_m	Pitching moment coefficient
D	Drag
D	In shorthand derivative notation $D_{(\ )} = \frac{1}{m} \frac{\partial D}{\partial (\ )}$
D	Aerodynamic time differential operator
I	Moment of inertia
IAS	Indicated airspeed
K_f	NACA emperical factor
L	Lift
L	In shorthand notation $L_{(\ )} = \frac{1}{m} \frac{\partial L}{\partial (\ )}$
L. E.	Wing leading edge
L_f	Overall fuselage length
M	Pitching moment + nose up
M	In shorthand derivative notation $M_{(\ )} = \frac{1}{Iy} \frac{\partial M}{\partial (\ )}$
N_o	Neutral point
N_m	Maneuver point
S	Wing area
S_t	Tail area
T	Thrust
TAS	True airspeed
$T_{\frac{1}{2}}$	Time to damp to $\frac{1}{2}$ initial amplitude
V	Velocity
$\overline{V}$	Tail volume coefficient
W	Weight

LIST OF SYMBOLS (Continued)

Small Letters

a	Lift curve slope
ac	Aerodynamic center
b	Span
$\bar{c}$	Wing mean aerodynamic chord
e	Span efficiency factor
g	Acceleration of gravity
h	Height of thrust line above CG
h	Altitude
i	Incidence angle
k	Radius of gyration
ℓ	Length in the X direction
m	Mass of the aircraft
mac	Mean aerodynamic chord
n	Load factor
q	Dynamic pressure
s	Laplace operator
t	Time
u	Non-dimensional velocity
w	Velocity along Z axis
w_f	Maximum width of the fuselage
$\bar{x}_a$	Non-dimensional distance wing ac ahead of CG
$\bar{x}_{CG}$	Non-dimensional distance CG aft of wing L. E.
y	Vertical distance of the tail quarter chord from the wing chord line + up

LIST OF SYMBOLS (Continued)

Subscripts

ac	Of or about the aerodynamic center
CG	Of the center of gravity
D	Of the propeller disc
e	Of the elevator
f	Of the fuselage
L	Of lift
s	Of the slipstream
t	Of the tail
y	Of or about the Y axis
o	Initial value
o	Two-dimensional
7.0	For inflation pressure of 7.0 psi
5.0	For inflation pressure of 5.0 psi

Greek

α	Angle of attack
δ	Control surface deflection angle + trailing edge up
Δ	Change in
ϵ	Downwash angle
η	Efficiency factor
λ	Characteristic root
λ	Taper ratio
Λ	Sweep angle
μ	Relative density factor
ω_n	Undamped natural frequency
ω_c	Damped frequency
ρ	Density
τ	Relative control effectiveness
τ	Aerodynamic time
θ	Pitch angle + nose up
ζ	Damping ratio

LIST OF SYMBOLS (Continued)

Derivatives (with respect to)

α	Angle of attack
$\dot{\alpha}$	Non-dimensional Angle of attack rate real time $\frac{\dot{\alpha}\bar{c}}{2V}$
$D\alpha$	Non-dimensional Angle of attack rate aerodynamic time
θ	Pitch angle
$\dot{\theta}$	Non-dimensional pitch rate real time
$D\theta$	Non-dimensional pitch rate aerodynamic time
δ_e	Elevator deflection
q	Non-dimensional pitch rate $\frac{\dot{\theta}\bar{c}}{2V}$
u	Non-dimensional
V	Forward velocity

SUMMARY

In January 1964 an investigation was begun to investigate the validity of classical rigid aircraft analytical techniques on predicting the stick fixed and dynamic longitudinal stability of the Goodyear YAO-3G Inflatoplane. In addition, a study was made on the effects of fuselage flexibility on the dynamic response in the phugoid mode and the movement of neutral and maneuver points.

It was found that rigid techniques were valid for dynamic response predictions and somewhat less valid for static predictions. However, if the airframe pressure was maintained at the designed level static predictions were in no way adverse. If the airframe is available for static bending test, correction factors may be obtained that when applied to rigid values of $C_{m_{i_t}}$ result in more accurate predictions of both dynamic and static stability.

Fuselage rigidity was varied by changing internal airframe pressure from 5 psig to 7 psig. The effect of fuselage flexibility was to reduce damping and increase the frequency of the phugoid mode to a slight extent. The neutral and maneuver points both moved forward; however, it was indicated that N_m moved further forward than N_o.

INTRODUCTION

The Goodyear YAO-3G is an aircraft that was developed in the 1950's and is no longer in production. The aircraft is unique in that it is of inflatable rubber-fabric construction.

In October of 1963 the Department of Aerospace and Mechanical Sciences of Princeton University obtained one of these aircraft on loan from the U. S. Army. It was determined that the unique features of the aircraft could be put to good use in an investigation of first order aeroelastic effects due to structural bending. The investigation would be simplified by the low aerodynamic pressure required to manifest such bending. In addition, the rigidity of the aircraft could be varied, within limits, by controlling the internal pressure of the airframe.

With these possibilities in mind this investigation was started in January of 1964. The first flight test was conducted on January 3, 1964 and the tests continued through early May of 1964.

The purpose of the investigation was twofold. First to investigate the validity of classical, rigid aircraft, analytical techniques in predicting static and dynamic longitudinal stability, and secondly to investigate the effects of fuselage and wing bending on the stick fixed maneuver and neutral points and the dynamic modes of longitudinal motion of this aircraft.

The investigation consisted of analytical developments considering the aircraft first rigid and then semi-rigid and comparing the analytical analysis with flight test results.

EQUIPMENT

The Aircraft

The YAO-3G is a single-placed high-wing monoplane of inflatable fabric construction (Figures 1 through 6 and Table I). The landing gear consists of a single fixed wheel with wing tip and tail skids. The aircraft is powered by a single engine driving a fixed pitch propeller. The engine is a Nelson Model H63-A which develops a maximum of 42 brake horsepower at 4000 RPM at sea level. The engine operates on the two-cycle principle, has a single magneto ignition, and air pump for controlling airframe pressure.

Other than being inflatable, the airframe is of conventional form consisting of a straight constant chord wing (NACA 0015), a fuselage with partially enclosed cockpit, and empennage with vertical and horizontal stabilizer and control surfaces. A conventional stick and rudder pedal control system is used for flight and manual control is provided for the engine mounted air pump and airframe pressure relief valve.

The rigidity of the aircraft is maintained by hoop stresses resulting from internal pressures varying from 4.8 to 7.0 psig. The shape of the non-cylindrical parts is maintained by drop stich threads running from one surface to the other as shown in Figure 6. The internal pressure changes with altitude and is maintained at the desired level by manipulation of the pump control and airframe pressure relief valve.

The instrumentation is quite basic consisting of an air speed indicator, altimeter, accelerometer, magnetic compass, air pressure gage, engine tachometer, and cylinder head temperature indicator (Figure 7). The electrical system consists of a dry cell battery powered warning light for the air pressure gage.

The basic weight of the aircraft was 315 pounds including test instrumentation and parachute. Gross weight varied from 500 to 600 pounds depending on pilot and fuel.

Flight Test Instrumentation

The instrumentation requirements were to provide the necessary data to perform static and dynamic longitudinal stability analyses. This required a method of measuring and recording elevator deflection, normal acceleration, airspeed, angle of attack, and pitch rate. In addition, a movie camera would be desirable to study fuselage bending during the phugoid motion, and voice communications requirements dictated self-contained radio equipment.

The instrumentation problems were somewhat different than would be expected of a more conventional aircraft. The space available for instrumentation was a small area behind the pilot on the cockpit floor. This space had to contain the major instrumentation components and power supply. Weight was also a problem in that a 200 pound pilot plus parachute and nominal fuel put the aircraft at near maximum gross weight. In addition, attachment points were limited and some method had to be devised to attach and remove instrumentation components without damage to the fabric airframe.

A SFIM A20 Flight Recorder was chosen to record data. This instrument is 6.5 x 4.7 x 3.9 inches and weighs 4.6 pounds including airspeed and acceleration transducers. A matched rate gyro 3 x 3 x 3 inches weighing 3 pounds was used to record pitch rate. Transducers in the recorder convert inputs to mirror deflections. The mirrors reflect light, from a single source, to light sensitive paper. Five input channels may be recorded on the 60 mm paper. The instrument and associated equipment draws 2 amps at 28 volts D.C.

The A20 can be set to run at tape speeds of 1 mm or 5 mm per second and holds approximately 25 feet of recording paper. To compensate for variations in tape speed with supply voltage, an internal clock mechanism is provided which projects time marks on the trace. In addition, a trace marking device is incorporated.

The recorder transducers consisted of an airspeed indicator that required static and dynamic pressure inputs, a self-contained accelerometer, two ratiometers, and a galvanometer for potentiometer inputs. The ratiometers compensate for variations in supply voltage and were used for pitch rate and elevator deflection inputs. The galvanometer is not insensitive to supply voltage and was used for the angle of attack input in that a qualitative value of angle of attack would be sufficient for the dynamic test. A more complete description of the SFIM A20 may be found in Reference 1.

The power supply consisted of 24 nickel cadmium batteries with a nominal output of 29 volts and capacity of 4 amp hours. The power supply was made up in two packs of 12 batteries each in order to better utilize space requirements.

The mounting problem was solved by the use of Permacel P69 fabric tape. This tape was found invaluable for manufacturing attachment points. It was found to adhere well through the various temperature and dynamic pressure conditions encounted during flight test.

Figure 8 shows the installation of the A20 recorder, rate gyro, and power supply.

In order to accurately measure elevator deflection, it was necessary to put a potentiometer on the elevator itself. Due to fuselage bending, the elevator could deflect with the stick fixed and cable measurement was not considered to be of sufficient accuracy. The potentiometer

mounting is shown in Figure 9. The potentiometer leads were taped to the fuselage right side. Due to the low dynamic pressure of the aircraft, external mountings were not a problem.

The mounting of the angle of attack vane presented a problem as to what part of the aircraft would be rigid enough to use as a reference. A typical wing mounted boom was out of the question due to wing twist and flexibility. As a compromise solution the boom was mounted by a two-foot bracket attached to the landing gear frame. The gear frame is the most rigid part of the aircraft; however, in order to preserve the rigidity of the mounting bracket, the boom had to be shorter than necessary to totally escape from wing interference. However, it was considered that the amount of wing interference encountered would not adversely affect angle of attack dynamic response. Although primarily designed as a mounting for the angle of attack vane, the mounting bracket seemed to be the ideal location for the movie camera (a surplus gun camera), also. Later on it was also used to mount a venturi tube. This venturi was necessary to amplify static pressure for the recorder airspeed transducer. The transducer was found to be insensitive at the low airspeeds encountered when attached to a simple pilot static tube. Figure 10 shows the angle of attack, camera, and venturi mounting.

A control panel for the recorder was mounted on the instrument panel in place of the magnetic compass (Figure 7). This panel contained a master switch to control power to the recorder motor and lamp, a speed switch that controlled the recorder motor, an event marker switch, and a five position selector switch and meter. The selector switch allowed the meter to read either elevator position, angle of attack, pitch rate, battery voltage, or off. This selector arrangement proved invaluable in that recorder inputs could be checked in flight. In addition, a switch panel was mounted on the right cockpit wall. This panel

contained angle of attack, pitch rate, and camera switches. The position of the angle of attack and pitch rate switches determined whether these values were being recorded. As these values were not necessary for the static test, their presence made trace reading more difficult. The switch panel allows static and dynamic tests to be conducted on the same flight without excessive traces on the tape. When the camera switch was on, the recorder motor switch also controlled the camera. An event marker switch was also mounted on the top of the pilot's control stick. Figure ~~4~~ 11 is a wiring diagram of the complete instrumentation package and Figure 12 is a schematic of the recorder system.

The voice communication system consisted of separate self-contained VHF transmitter and receiver. The transmitter was a Navguide Corporation Model AT-103 which was 5 x 7 x 2 inches and weighed 5 pounds including batteries. The Navguide is a crystal tuned 5 tube VHF transmitter which operates on dry cells. The filaments do not light until the microphone button is depressed. It was found that the filament battery would not sustain semi-continuous operation necessary during flight test. To aleviate this the recorder power supply was put in parallel with the filament battery after being dropped down to 14 volts with a 4000 ohm, 5 watt resistor. The transmitter was mounted behind the pilot just under the leading edge of the wing. The transmitter antenna was taped to the left outer cockpit wall (Figure 3). The receiver was a Montery Electronics "Partner" continuous tuning VHF receiver 2 x 4 x 5 inches weighing $1\frac{1}{2}$ pounds including mercury batteries. The receiver was mounted on the left inner cockpit wall (Figure 7). The receiver antenna was taped to the left outer cockpit wall (Figure 3).

As the aircraft has no metal skin there was no ground plane effect for the antenna mountings and the receiver would not operate under these

conditions. A ground plane was constructed from 1/16 inch welding rod and taped to the underside of the cockpit. This arrangement proved quite satisfactory for two way communication up to 5 miles. As this range was satisfactory for flight test no ground plane was used for the transmitter antenna.

The total weight of the instrumentation including all mountings amounted to 33.5 pounds. The SFIM recorder operated very well throughout the flight test. Its light weight, compact size, and simple power supply requirement solved the basic instrumentation problem.

ANALYTICAL PROCEDURES

Longitudinal Stick-fixed Stability

The longitudinal stability is determined by considering the motion of the aircraft in horizontal and vertical translation and in pitch. Symmetry of the aircraft precludes any coupling between longitudinal and lateral motions. The wind-axis is assumed to be parallel to the principal longitudinal axis in the vertical plane of symmetry, thus eliminating the products of inertia. The resulting perturbation equations of motion are, from Reference 2.

$$\Delta\dot{V} + (D_V - T'_V)\Delta V + (D_\alpha - g)\Delta\alpha + g\Delta\theta = 0$$

$$\frac{L_V}{V_o}\Delta V + \Delta\dot{\alpha} + \frac{L_\alpha}{V_o}\Delta\alpha - \Delta\dot{\theta} = 0$$

$$- M_V\Delta V - M_{\dot{\alpha}}\Delta\alpha - M_\alpha\Delta\alpha + \Delta\ddot{\theta} - M_{\dot{\theta}}\Delta\dot{\theta} = M_{\delta_e}\Delta\delta_e$$

In this evaluation the aircraft will be considered as a rigid body except where full-scale wind tunnel test data is available. Using the aircraft specifications of Table I and references as noted, the stability derivatives may be evaluated as follows. The flight conditions used for evaluation will be:

$W = 515.2$ lbs.
c.g. = 29% mac
$h =$ sea level
$V = 50$ knots $= 84.45$ fps

The lift coefficient is determined from:

$$C_L = \frac{2L}{\rho V^2 S} = \frac{(2)(515.2)}{(.00238)(84.45)^2(124.3)}$$

$$C_L = .488$$

The drag coefficient is determined from:

$$C_D = C_{D_o} + \frac{C_L^2}{e\pi AR}$$

With $C_{D_o} = .1$ from Reference 3, and a reasonable value of the aircraft efficiency factor, e, taken as .75, the drag coefficient becomes:

$$C_D = .1 + \frac{(.488)^2}{(.75)(3.14)(4.44)}$$

$$C_D = .123$$

The aircraft non-dimensional mass based on wing chord is:

$$\mu = \frac{m}{\rho S\bar{c}} = \frac{16}{(.00238)(124.3)(5.31)} = 10.28$$

The effect on the forces and moments due to a change in forward speed with angle of attack and throttle fixed are stated below. Drag changes with speed by:

$$D_V = \frac{\rho S V}{m} C_D = \frac{(.00238)(124.3)(84.45)(.123)}{16}$$

$$D_V = .1915$$

The thrust versus velocity curve shown in Reference 3, gives a change of thrust with velocity of -.711 lbs/ft/sec.

$$T_V = \frac{1}{m}\frac{dT}{dV} = \frac{-.711}{16}$$

$$T_V = -.04445$$

The change of lift with a change of velocity is expressible by:

$$\frac{L_V}{V_o} = \frac{2g}{V^2} = \frac{(2)(32.2)}{(84.45)^2}$$

$$\frac{L_V}{V_o} = .00903$$

With the engine lever arm 3.14' above the center of gravity and assuming the thrust line parallel to the fuselage reference line, the change in pitching moment with speed is:

$$M_V = \frac{1}{Iy}\frac{\partial M}{\partial V} = \frac{1}{Iy}\frac{\partial T}{\partial V} h = \frac{(-.711)(-3.14)}{277.2}$$

$$M_V = .00806$$

The changes that occur in the forces and moments with a change in angle of attack are normally an increase in lift, an increase in drag and a negative pitching moment. The lift curve slope of the aircraft at 50 knots as determined from full-scale wind tunnel tests, Reference 4, is:

$$C_{L_\alpha} = 4.18 \ /\mathrm{rad}$$

The drag change with angle of attack is represented by:

$$D_\alpha = \frac{2g}{e\pi AR} C_{L_\alpha} = \frac{(2)(32.2)(4.18)}{(.75)(3.14)(4.44)}$$

$$D_\alpha = 26.0$$

A change in angle of attack effects the lift by:

$$\frac{L_\alpha}{V_o} = \frac{gC_{L_\alpha}}{C_L V_o} = \frac{(32.2)(4.18)}{(.488)(84.45)}$$

$$\frac{L_\alpha}{V_o} = 3.265$$

In determining the angle of attack effect on the pitching moment the contributions of the fuselage and tail must be considered first. The fuselage contribution may be estimated from Reference 5 by:

$$C_{m_{\alpha_f}} = \frac{K_f W_f^2 L_f}{S\bar{c}}$$

Where L_f is the overall fuselage length, W_f is the maximum width of the fuselage, and K_f is an emperical factor determined from experimental evidence.

$$C_{m_{\alpha f}} = \frac{(.012)(2.25)^2(19.6)}{(124.3)(5.31)} = .0184$$

An angle of attack change at the tail produces a moment change as follows:

$$C_{m_{i_t}} = C_{m_{\alpha_t}} = -a_t \, \eta_t \, \bar{V}_t$$

The tail efficiency, $\eta_t = \frac{qt}{q}$ is felt to be about 1.3 due to slipstream effect. This value was verified experimentally as described in the test procedures section and found to be a reasonable assumption. The lift curve slope of the tail can be estimated from Reference 6 to be, $a_t = 2.7/\text{rad}$.

$$C_{m_{i_t}} = -(2.7)(1.3)(.399) = -1.397$$

A lag in the downwash reaching the tail may be found from the emperically determined formula: (Reference 14)

$$\frac{d\epsilon}{d\alpha} = \frac{C_{L_\alpha} 27 \cos^{3/2} \Lambda}{57.3\,(.525 + .475\lambda^{.736})AR^{.725}(\frac{\ell_t}{\bar{c}})^{.2} e^{.385\, y/\bar{c}}}$$

Where y is the vertical distance of the tail quarter chord from the wing chord line (+ above).

$$\frac{d\epsilon}{d\alpha} = \frac{(4.18)(27)}{(57.3)(4.44)^{.725}(2.345)^{.2}e^{.0806}}$$

$y = 1.0$

$\Lambda = 0$

$\lambda = 1.0$

$$\frac{d\epsilon}{d\alpha} = .42$$

Now the moment change with angle of attack change may be computed by:

$$M_\alpha = \frac{g}{\bar{c}\, C_L \left(\frac{by}{\bar{c}}\right)^2} C_{m_\alpha}$$

where

$$C_{m_\alpha} = C_{L_\alpha} \bar{x}_a + C_{m_{\alpha_f}} + C_{m_{i_t}}\left(1 - \frac{d\epsilon}{d\alpha}\right)$$

$$C_{m_\alpha} = (4.18)(.04) + .0184 - 1.397\,(1 - .42)$$

$$C_{m_\alpha} = -.6247$$

$$M_\alpha = \frac{(32.2)(-.6247)}{(5.31)(.488)(.615)}$$

$$M_\alpha = -12.61$$

There is also a moment change due to rate of change of angle of attack given by:

$$M_{\dot{\alpha}} = \frac{g}{VC_L(\frac{ky}{\bar{c}})^2} \frac{\ell_t}{\bar{c}} \frac{d\epsilon}{d\alpha} C_{m_{i_t}}$$

$$M_{\dot{\alpha}} = \frac{(32.2)(2.345)(.42)(-1.397)}{(84.45)(.488)(.615)}$$

$$M_{\dot{\alpha}} = -1.746$$

The principal effect of pitch is manifested in a damping of the moment as follows:

$$M_{\dot{\theta}} = \frac{M_{\dot{\alpha}}}{\frac{d\epsilon}{d\alpha}} = \frac{-1.748}{.42}$$

$$M_{\dot{\theta}} = -4.16$$

The elevator control power may be expressed by:

$$M_{\delta_e} = \frac{g}{C_L\,\bar{c}\,(\frac{ky}{\bar{c}})^2} \tau_e C_{m_{i_t}}$$

where τ_e, the control effectiveness parameter, is .6 from Figure 5-33 of Reference 7.

$$M_{\delta_e} = \frac{(32.2)(.6)(-1.397)}{(.488)(5.31)(.615)}$$

$$M_{\delta_e} = -16.82$$

Using the stability derivatives above, the following determinant of coefficients is obtained:

$$\left|\begin{array}{ccc} \Delta V & \Delta\alpha & \Delta\theta \\ s + .236 & -6.2 & 32.2 \\ .00903 & s + 3.265 & -s \\ -.00806 & 1.746s + 12.61 & s(s+4.16) \end{array}\right| = 0$$

From this the characteristic equation for the rigid aircraft is:

$$\lambda^4 + 9.407\lambda^3 + 28.4124\lambda^2 + 7.1315\lambda + 4.514 = 0$$

Solution of the equation yields phugoid and short period characteristics of:

Phugoid	Short Period
$\zeta = .245$	$\zeta = .897$
$\omega n = .414$	$\omega n = 5.128$
$T\frac{1}{2} = 7.05$ sec	$T\frac{1}{2} = .151$ sec
Period = 15.7 sec	Period = 1.22 sec
$\omega c = .401$	$\omega c = 2.28$

Static Stability

The neutral point and maneuver point for the rigid aircraft can be determined from the stability derivatives once they have been converted to non-dimensional form.

$$N_o - x_{cg} = -\frac{C_{m_\alpha}}{C_{L_\alpha}} + \frac{C_{m_u}}{2C_L}$$

$$N_m - x_{cg} = -\frac{C_{m_\alpha}}{C_{L_\alpha}} - \frac{C_{m_{D\theta}}}{2}$$

$C_{m_\alpha} = -.6247$

$C_{m_u} = .0342$

$C_{m_{D\theta}} = -.3187$

$C_{L_\alpha} = 4.18$

$x_{cg} = .29$

The resulting stick-fixed neutral and maneuver points are:

$N_o = 47.5\%$ mac

$N_m = 59.9\%$ mac

The slope of the neutral point curve may be determined by differentiating $\frac{d\delta_e}{dC_L}$ by x_{cg}.

$$\frac{d\delta_e}{dC_L} = \frac{d\delta_e}{dC_m}\,\frac{dC_m}{dC_L} = \frac{dC_m}{dC_L}\,\frac{1}{C_{m_\delta}}$$

$$= \frac{1}{C_{m_\delta}}\left(\frac{C_{m_\alpha}}{C_{L_\alpha}} + \frac{C_{m_V}}{C_{L_V}}\right)$$

$$= \frac{1}{C_{m_\delta}}\left(\frac{C_{m_\alpha}}{C_{L_\alpha}} - \frac{C_{m_u}}{2C_L}\right)$$

$$= \frac{1}{C_{m_\delta}}\left[\frac{C_{L_\alpha}(x_{cg} - x_{ac}) + C_{m_{\alpha_f}} + C_{m_{i_t}}(1 - \frac{d\epsilon}{d\alpha})}{C_{L_\alpha}} - \frac{C_{m_u}}{2C_L}\right]$$

$$d\left(\frac{d\delta_e}{dC_L}\right)\Big/dx_{cg} = \frac{1}{C_{m_\delta}} = \frac{1}{\tau_e\, C_{m_{i_t}}}$$

With the elevator effectiveness estimated as, $\tau_e = .6$, the slope of the neutral point curve is:

$$d\left(\frac{d\delta_e}{dC_L}\right)\Big/dx_{cg} = -1.191$$

The slope of the maneuver point curve may likewise be determined by differentiating $\frac{d\delta_e}{dn}$ with respect to x_{cg}.

$$\frac{d\delta_e}{dn} = \frac{d\delta_e}{dC_m}\,\frac{dC_m}{dn} = \frac{d\delta_e}{dC_m}\,\frac{dC_m}{d\,\frac{L}{W}}$$

$$= \frac{W}{C_{m_\delta}}\,\frac{dC_m}{dL} = \frac{W}{C_{m_\delta}}\,\frac{dC_m}{dC_L}\,\frac{1}{qS}$$

$$= \frac{C_{L_{n=1}}}{C_{m_\delta}}\left[\frac{C_{L_\alpha}(x_{cg} - x_{ac}) + C_{m_{\alpha_f}} + C_{m_{i_t}}\left(1 - \frac{d\varepsilon}{d\alpha}\right)}{C_{L_\alpha}}\right]$$

$$d\left(\frac{d\delta_e}{dn}\right)\Big/ dx_{cg} = \frac{C_{L_{n=1}}}{C_{m_\delta}} = \frac{C_{L_{n=1}}}{\tau_e\, C_{m_{i_t}}}$$

The slope of the maneuver point curve for the rigid case is:

$$d\left(\frac{d\delta_e}{dn}\right)\Big/ dx_{cg} = -.581$$

Analog Computer and Root Locus

Due to the flexibility of this aircraft, the vertical bending of the rear portion of the fuselage will manifest itself in a change in the horizontal stabilizer incidence, i_t. This change can be considered as a change in the derivative $C_{m_{i_t}}$. This effect has serious aerodynamic consequences because all the pitching moment stability derivatives, with the exception of speed stability, are a function of $C_{m_{i_t}}$.

The effect of wing bending predominately manifests itself in a change in C_{L_α}. In this investigation a varying C_{L_α} will be used.

In order to observe the result of varying tail incidence, $C_{m_{i_t}}$ was factored out of the moment equation.

$$-V_o M_V \Delta u - M_{\dot{\alpha}} \Delta\dot{\alpha} - M_\alpha \Delta\alpha + \Delta\ddot{\theta} - M_{\dot{\theta}} \Delta\dot{\theta} - M_{\delta_e} \Delta\delta_e = 0$$

$$-V_o M_V \Delta u - \left\{ \frac{g}{V C_L \left(\frac{ky}{\bar{c}}\right)^2} \frac{\ell_t}{\bar{c}} \frac{d\epsilon}{d\alpha} C_{m_{i_t}} \right\} \Delta\dot{\alpha}$$

$$-\frac{g}{\bar{c} C_L \left(\frac{ky}{\bar{c}}\right)^2} \left\{ a_w \bar{x}_a + C_{m_{\alpha_f}} + C_{m_{i_t}} \left(1 - \frac{d\epsilon}{d\alpha}\right) \right\}$$

$$+\Delta\ddot{\theta} - \left\{ \frac{g}{V C_L \left(\frac{ky}{\bar{c}}\right)^2} \frac{\ell_t}{\bar{c}} C_{m_{i_t}} \right\} \Delta\dot{\theta} - \left\{ \frac{g}{V C_L \left(\frac{ky}{\bar{c}}\right)^2} \tau_e C_{m_{i_t}} \right\} = 0$$

$$-\Delta\ddot{\theta} = -V_o M_V \Delta u - \frac{g}{C_L \bar{c} \left(\frac{ky}{\bar{c}}\right)^2} \left[a_w \bar{x}_a + C_{m_{\alpha_f}} \right] \Delta\alpha$$

$$-\frac{g}{C_L \bar{c} \left(\frac{ky}{\bar{c}}\right)^2} C_{m_{i_t}} \left\{ \left(\frac{\ell_t}{V} \frac{d\epsilon}{d\alpha}\right) \Delta\dot{\alpha} + \left(1 - \frac{d\epsilon}{d\alpha}\right) \Delta\alpha + \frac{\ell_t}{V} \Delta\dot{\theta} + \tau_e \Delta\delta_e \right\}$$

This leaves the moment equation in a suitable form for both root locus and analog simulation.

The root locus equation for varying $C_{m_{i_t}}$ was derived from the following determinant where $\frac{K}{2} = \frac{g}{C_L \bar{c} \left(\frac{ky}{\bar{c}}\right)^2}$

$$\begin{vmatrix} s + (D_V - T_V) & \frac{D_\alpha - g}{V_o} & \frac{g}{V_o} \\ L_V & s + \frac{L_\alpha}{V_o} & -s \\ -V_o M_V & -\frac{K}{2}\left\{C_{L_\alpha} x_\alpha + C_{m_{\alpha_f}} + C_{m_{i_t}}\left[\frac{\ell_t}{V}\frac{d\varepsilon}{d\alpha} s + \left(1 - \frac{d\varepsilon}{d\alpha}\right)\right]\right\} & s\left(s - \frac{K}{2}\frac{\ell_t}{V} C_{m_{i_t}}\right) \end{vmatrix}$$

Upon substituting into the above determinant for all values except C_{L_α} and $C_{m_{i_t}}$, the following determinant was formed.

$$\begin{vmatrix} s + .236 & (.0736\, C_{L_\alpha} - .3815) & + .3815 \\ .761 & s + .781\, C_{L_\alpha} & -s \\ -.681 & \left\{.814\, C_{L_\alpha} - .3625 - C_{m_{i_t}}\left[1.251\, s + 11.69\right]\right\} & s(s - 2.977\, C_{m_{i_t}}) \end{vmatrix}$$

This produced the following root locus equation for a varying $C_{m_{i_t}}$

$$\frac{4.238\left|C_{m_{i_t}}\right|[s^3+(2.9943+.5486C_{L_\alpha})s^2+(.9406+.0901\,C_{L_\alpha})s+.8008]}{s^4+(.236+.781C_{L_\alpha})s^3+(-.0722-.6777C_{L_\alpha})s^2+(-.0855-.14C_{L_\alpha})s+(-.1052-.0292C_{L_\alpha})} = -1$$

C_{L_α} was not substituted in because the root locus will be drawn for a range of C_{L_α}'s. This procedure was used because C_{L_α} has a large effect on the dynamics of the aircraft. Also the variable C_{L_α} obtained from Reference 3 could not be depended on since the configurations do not match exactly. The root locus will be drawn for a range of possible C_{L_α}'s, C_{L_α} = 3.0, 4.0, and 5.0 per radian.

$\underline{C_{L_\alpha} = 3.0}$

$$\frac{4.238\left|C_{m_{i_t}}\right|[s^3+4.6401s^2+1.2110s+.8008]}{s^4+2.579s^3-2.1053s^2-.5055s-.1925} = -1$$

$$\frac{4.238\left|C_{m_{i_t}}\right|(s+4.4065)(s+.1168\pm j\,.4099)}{(s+3.1941)(s-.8591)(s+.122\pm j\,.2351)} = -1$$

$C_{L_\alpha} = 4.0$

$$\frac{4.238\left|C_{m_{i_t}}\right|(s^3 + 5.1887s^2 + 1.3012s + .8008)}{s^4 + 3.36s^3 - 2.783s^2 - .6455s - .2216} = -1$$

$$\frac{4.238\left|C_{m_{i_t}}\right|(s + 4.9588)(s + .1149 \pm j\,.3852)}{(s + 4.0166)(s - .8906)(s + .117 \pm j\,.2197)} = -1$$

$C_{L_\alpha} = 5.0$

$$\frac{4.238\left|C_{m_{i_t}}\right|(s^3 + 5.7373s^2 + 1.3913s + .8008)}{s^4 + 4.141s^3 - 3.4607s^2 - .7855s - .2507} = -1$$

$$\frac{4.238\left|C_{m_{i_t}}\right|(s + 5.5112)(s + .1131 \pm j\,.357)}{(s + 4.8268)(s - .9143)(s + .1143 \pm j\,.2092)} = -1$$

The root locus for varying $C_{m_{i_t}}$ for the three C_{L_α}'s is shown in Figure 16. Figure 17 shows the stable phugoid portion of Figure 16 with an expanded scale. Lines of constant $C_{m_{i_t}}$ are shown plotted on these curves. Figure 17 also shows lines of constant damping ratio, ζ.

The analog simulation was based on the normal lift and drag equations plus the modified moment equation. The equations used in the analog simulation are shown on the following page.

$$-\Delta\dot{\theta} = -\int\{V_o M_V \Delta u + \frac{K}{2}\bar{x}_a C_{L_\alpha} \Delta\alpha + \frac{K}{2} C_{m_{\alpha_f}} \Delta\alpha - \frac{C_{m_{i_t}}}{2} P\}\, dt$$

$$-P = -\Sigma[K\frac{\ell_t}{V_o}\frac{d\epsilon}{d\alpha}\Delta\dot{\alpha} + K(1-\frac{d\epsilon}{d\alpha})\Delta\alpha + K\frac{\ell_t}{V_o}\Delta\dot{\theta} + K\tau_e\Delta\delta_e]$$

$$\Delta u = -\int\{D_V - T_V)\Delta u + \frac{2g}{V_o e\pi AR} C_{L_\alpha}\Delta\alpha - \frac{g}{V_o}\Delta\alpha + \frac{g}{V_o}\Delta\theta\}\, dt$$

$$\Delta\dot{\alpha} = -\Sigma L_V \Delta u + \frac{g}{C_L V_o} C_{L_\alpha}\Delta\alpha - \Delta\dot{\theta}$$

$$-\Delta h = -\int\{V_o\Delta\theta - V_o\Delta\alpha\}\, dt$$

Figure 13 shows the computer set-up used. Table II is a tabulation of the pots versus the quantity they set. The computer set-up was made in such a way as to keep C_{L_α} and $C_{m_{i_t}}$ separate. This could be accomplished easily for $C_{m_{i_t}}$ by taking advantage of the previously factored equations. However, the C_{L_α} could not be so easily separated since it enters the lift, drag, and moment equations.

The computer set-up was checked by comparing the analytic solution with the computer solution. This Sanborn tape is shown in Figure 14. As can be seen in Figure 17, the computer solution plots very close to the analytic solution.

Analog computer runs were made for C_{L_α}'s of 3.0, 4.0 and 5.0 per radian. $C_{m_{i_t}}$ was varied from 2.0 down to the $C_{m_{i_t}}$ for critical damping. Typical Sanborn tapes are shown in Figure 15.

Agreement between the root locus and the analog computer was checked by making analog runs at C_{L_α}'s of 3.0, 4.0, and 5.0 per radian and with $C_{m_{i_t}} = 1.0$. The ω_c's were taken directly from the tapes while the ζ's were found by taking amplitude ratios from the tapes and applying them to Figure 18. These values are shown plotted on Figure 17.

All analog runs are for a δ_e of .15 radians introduced as a pulse of about 3 seconds duration.

FLIGHT TEST PROCEDURES

The flight test phase of the investigation began in January 1964 and continued through early May 1964 consisting of 33 hours of flight time. These tests were conducted at the air facility at the Forrestal Research Center of Princeton University. This phase consisted of preflight calibrations, in-flight calibrations, stick fixed longitudinal static stability flight test, stick fixed longitudinal dynamic stability flight test, flight test determination of pitching moment due to tail angle of attack ($C_{m_{i_t}}$), and elevator effectiveness (τ_e).

Preflight Calibrations

As soon as the test instrumentation was installed the aircraft was weighed with various fuel loads to determine fuel weight and moment contributions. The aircraft was then weighed with no fuel and each of the three pilots. The fuel weight and moment were then added to pilot weight and moment to arrive at center of gravity locations and gross weight versus fuel load (Figure 19).

It was found that three pilots weighing 170 lbs., 190 lbs, and 210 lbs., respectively, produced center of gravity excursions from 24.10% MAC to 30.00% MAC. An attempt was made to extend this range of center of gravity locations aft by adding weights to the tail; however, this introduced nonlinearities in fuselage bending that could not be accounted for in the static stability test. It was decided that with a large selection of flight test points the static stability curves could be accurately extrapolated with the center of gravity excursion provided by different pilots.

The elevator motion was calibrated by attaching a protractor to the elevator and recording deflections obtained by selecting control

stick positions. This calibration was found to be different for 7 psi and 5 psi internal pressures. As elevator calibration was critical for static stability tests, the elevator calibration was done every time flight test data was obtained. A possible explanation for the change of elevator calibration is that the string attached to the potentiometer could change length due to aging and ambient weather conditions. The use of wire would eliminate the problem, but was ruled out for flight safety reasons. A string was chosen instead of a wire to preclude the possible jamming of the control system by the instrumentation.

The only calibration required of the angle of attack vane was to assure that its nominal position fell in the center of the recorder trace as no quantitative results were required of it.

The recorder accelerometer was simply recorded at +1 and -1 *g* in order to check the flight test calibration for a 2 *g* range.

In predicting $C_{m_{i_t}}$ for the analytical development it was necessary to choose a value for tail efficiency (η_t). It was felt that η_t for this aircraft would be greater than 1.0 because there are no fuselage effects to dissipate the wake other than that obtained by the downwash effect off the wing lowering it into the fuselage. Considering no downwash effect the following development was made:

From the momentum theory:

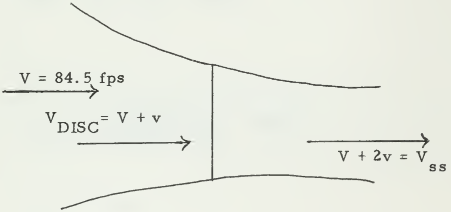

(1) $V_{disc} = V + v$

where v is velocity induced by disc at the disc

(2) $V_{ss} = V + 2v$ (downstream)

Therefore mass flow = $\rho A_D(V + v)$

and from (2):

$$v = \frac{V_{ss} - V}{2}$$

Therefore:

$$\text{mass flow} = \frac{\rho A_D}{2}(V_{ss} + V)$$

and

$$\text{Thrust} = (\rho A_D \, V_D)2v$$

$$T = \frac{\rho A_D}{2}(V_{ss} + V)(V_{ss} - V)$$

or:

$$V_{ss} = \frac{2T}{\rho A_D} + V^2$$

and from the analytical development made at test conditions, i.e., V = 54 knots IAS

$$\text{Drag} = 129.4 \text{ lbs} = \text{Thrust}$$

Therefore:

$$V_{ss} = \sqrt{\frac{(2)(129.4)}{(0.0024)(12.02)} + (84.5)^2}$$

$$V_{ss} = 127 \text{ fps}$$

Therefore from (2):

$$2v = 42.5 \text{ fps}$$

Therefore if no downwash effect is considered and accepting the assumptions that went into the momentum theory (i. e., constant v across disc, etc.), the difference between the velocity in the wake and the free stream should be 42.5 fps. Assuming this the case, the engine was run statically and power adjusted to produce maximum wake velocities of 40, 45, and 50 fps. These surveys were made with a velometer, which is a mass flow device. At these power settings wake surveys were made at the tail with the velometer and average tail velocities plotted versus wake velocity on Figure 20.

Entering Figure 20 with wake velocity of 42.5 fps an average tail velocity of 31.2 fps was obtained. This velocity is then the prop wake contribution to tail velocity at the flight condition. From this tail efficiency was calculated as follows:

$$\eta_t = \frac{q_t}{q} = \frac{(84.5 + 31.2)^2}{(84.5)^2}$$

$$\eta_t = 1.88$$

This figure is most idealized in that many assumptions were necessary to obtain it; however, it does justify values of η_t greater than 1.0. If the downwash effect is considered an $\eta_t = 1.3$ is not considered to be out of order. Consequently, this value was used in the analytical development.

It was also necessary to estimate the change in $C_{m_{i_t}}$ due to fuselage bending. The aircraft was suspended and a 25 lb weight placed on

the tail. At internal pressures of 5 psig and 7 psig the deflection of the tail relative to the wing root chord was found to be 1.8 degrees for 5 psig and 0.9 degrees for 7 psig internal pressure. Therefore:

$$\left.\frac{\Delta\alpha_t}{\text{lb.f}}\right)_{7.0} = \frac{0.9}{25} = \frac{1}{27.8} \text{ deg/lb.f}$$

$$\left.\frac{\Delta\alpha_t}{\text{lb.f}}\right)_{5.0} = \frac{1}{13.9} \text{ deg/lb.f}$$

Then for any change in force on tail ΔF:

$$\Delta\alpha_t)_{7.0} = \frac{\Delta F}{27.8} \text{ deg}$$

$$\Delta\alpha_t)_{5.0} = \frac{\Delta F}{13.9} \text{ deg}$$

or:

$$\underset{\text{due to bending}}{\Delta\alpha_t} = \frac{\Delta F}{K}$$

Knowing ~~α_t~~ ∂_r and q (8.46 psf at S. L.) a change in α_t of 1 degree will result in a change in force on the rigid tail of 8.4 lb.f.

Therefore:

$$\Delta F = 8.4\ \Delta\alpha_t$$

Now, the change in angle of attack of the tail due to the flexible fuselage may be expressed as:

$$\Delta\alpha_t = \Delta\alpha_{t_{\text{rigid}}} - \Delta\alpha_{t_{\text{due to bending}}}$$

or:

$$\Delta\alpha_t + \frac{\Delta F}{K} = \Delta\alpha_{t_{\text{rigid}}}$$

and:

$$\Delta\alpha_t + \frac{8.4}{K}\Delta\alpha_t = \Delta\alpha_{t_{\text{rigid}}}$$

Solving for $\Delta\alpha_t$:

$$\Delta\alpha_t = \left(\frac{K}{K + 8.4}\right)\Delta\alpha_{t_{\text{rigid}}}$$

Since $C_{m_{i_t}}$ varies directly with $\Delta\alpha_t$ and substituting for values of K found previously:

$$\left.C_{m_{i_t}}\right)_{7.0} = 0.768 \left.C_{m_{i_t}}\right)_{\text{rigid}}$$

$$\left.C_{m_{i_t}}\right)_{5.0} = 0.623 \left.C_{m_{i_t}}\right)_{\text{rigid}}$$

From analytical development $C_{m_{i_t}}\big)_{rigid} = 1.397$
Therefore:

$$C_{m_{i_t}}\Big)_{7.0} = 1.075$$

$$C_{m_{i_t}}\Big)_{5.0} = 0.871$$

These values will be compared with other methods of $C_{m_{i_t}}$ determination in the results section of the report.

Flight Calibrations

The in-flight calibrations consisted of airspeed and normal acceleration calibrations. The cockpit airspeed indicator calibration was obtained by flying the aircraft at approximately 20 feet above the runway at indicated airspeeds of 45, 50, 55, 60, and 65 knots. These runs were made on reciprocal runway headings in order to compensate for wind. Knowing the runway length the average time for each run enabled a true airspeed calculation. This true airspeed was then corrected for temperature and pressure altitude to obtain calibrated or corrected indicated airspeed. The results of the calibration are shown in Figure 21. Calibrations were run on January 3rd, January 7th, and April 25th with agreement on all three dates. The recorder airspeed indicator was calibrated against the cockpit indicator. However, as mentioned previously, the static source for the recorder airspeed indicator was a venturi mounted on the angle of attack boom mount. The aircraft pilot static tube was used as the dynamic pressure source for each instrument.

The recorder accelerometer calibration was obtained by readings made of two cockpit accelerometers in steady turns. The aircraft was

equipped with a standard cockpit accelerometer and a glass tube accelerometer was also added as a check. The two instruments were in agreement and the calibration of the recorder accelerometer did not change throughout the flight test.

Flight Test of Stick Fixed Static Stability

The static stability tests were conducted at a power setting to give 54 knot IAS in level flight. (This was the condition used in the dynamic analysis.) This power setting was held constant for all flight tests.

An accurate record of fuel on ~~hand~~ board was kept in order to know weight and center of gravity location for calculation of lift coefficients and correcting normal acceleration to a standard gross weight. Fuel was measured at the beginning and end of each flight. A consumption rate of 4 gallons (24 lbs) per hour was obtained and this rate was used to calculate fuel on board for each recorded event.

Determination of Stick Fixed Neutral Points

Neutral points were obtained for internal pressures of 7.0 and 5.0 psig. The flight procedure was to set the power at 54 knots IAS in level flight. Elevator deflection and airspeed were then recorded at indicated airspeeds of 45, 50, 55, and 60 knots after a steady state flight condition had been reached. These runs were repeated by each pilot to obtain data at three different center of gravity locations.

For the 7 psig runs an additional point was taken at 65 knots IAS, however, at 5 psig an undamped high frequency oscillation was encountered at 63 knots IAS. An explanation of this motion is presented in the Discussion of Results. Figure 22 shows a typical trace for elevator versus airspeed and also a trace of the oscillation.

Elevator deflection was then plotted versus lift coefficient for each center of gravity location. These plots were linear and the slopes, δ_e / C_L, were plotted versus center of gravity location to obtain neutral point. Figures 23 through 29 show the plots of δ_e versus C_L and Figures 30, ~~31,~~ and 32 show plots of δ_e / C_L versus X_{cg} for 5 psig, 7 psig, and rigid calculations.

Determination of Stick Fixed Maneuver Points

Maneuver points were also obtained for internal pressures of 5.0 psig and 7.0 psig. For these test power was set at 54 knots IAS in level flight. The aircraft was then slowed to 45 knots IAS and pushed over to obtain 57 knots IAS. A pull up was then initiated with a constant elevator position. During the pull up airspeed, normal acceleration, and elevator position were recorded. The tests were repeated for each center of gravity location. At the point on the trace where the airspeed was 54 knots IAS, acceleration and elevator positions were read and plotted on Figures 23 through 29. Figure 22 shows a typical trace of δ_e, V, and n. The normal acceleration was corrected to a standard gross weight of 515 ~~520~~ lbs in order to match the flight condition used for the dynamic calculations (i.e., 515 ~~520~~ lbs gross weight, center of gravity at 29.00% MAC, and 54.0 knots IAS). The plots of δ_e versus n were linear up to approximately 2 g's. At load factors above this the fuselage bending became nonlinear. However, since the dynamic motion was later found to be in the linear region, these linear slopes were used for plotting $d\delta_e / dn$ versus X_{cg} to obtain maneuver points. Figures ~~30,~~ 31, and 32 show plots of $d\delta_e / dn$ versus X_{cg} for 5 psig, 7 psig, and rigid calculations.

Determination of Longitudinal Stick Fixed Dynamic Stability

Dynamic tests were conducted at 5 psig and 7 psig internal pressures. For the dynamic test the aircraft was loaded so as to obtain a gross weight of ~~520~~ 515 lbs and a center of gravity location of 29.00% MAC in order to match the condition of the analytical development.

The aircraft was excited with a pulse elevator input. It was found that some method of returning the pulse to the original amplitude and holding it there was necessary. In order to achieve this a chord was attached to the pilot's lap belt and to a ring that could be slipped over the control stick. The length of the chord was adjusted to maintain 54 knots IAS in level flight. After each pull up the control stick was held against the chord to obtain a constant elevator deflection. This sort of "Rube Goldberg" arrangement is typical of what must be resorted to when an airframe will not accept screws or nuts and bolts graciously.

During the dynamic test elevator deflection, airspeed, angle of attack, pitch rate, and acceleration were recorded. Figure 33 is a typical recorder trace showing the dynamic response.

In addition, during some of the tests the gun camera recorded fuselage deflection during the phugoid motion. A flutter of the elevator was used to correlate events on the camera and the recorder trace. From the recorder trace phugoid damping ratio (ζ) was computed by Figure 18. Damping ratio and frequency of phugoid oscillation (ω_c) were then plotted on Figure 17 which is a root locus plot obtained from the analytical development.

The short period oscillation was not investigated. The analytical development indicated at short period time constant of the order of 0.2 seconds. The angle of attack vane would not respond at this rate and from matching elevator input and angle of attack response it is impossible to

differentiate between aircraft short period and angle of attack vane response. In any event, the highly damped short period mode was not considered interesting enough to warrent a more intense investigation.

Movie shots of fuselage bending were projected on a grid screen. From these observations it was possible to determine fuselage bending, in inches, at the tail and where in the motion the bending occurred. From the preflight test calibrations it was determined that the maximum bending for the 5 psig runs was of the order of 1.5 degrees, and 1.0 degrees at 7.0 psig. This order of bending agrees with the magnitudes found in the preflight test determination of $C_{m_{i_t}}$ by statically bending the fuselage. Figure 34 shows three typical frames from the movie shots.

Determination of $C_{m_{i_t}}$ and τ_e

In order to further verify the analytical development it was necessary to find the aircraft pitching moment due to tail incidence change ($C_{m_{i_t}}$) and elevator effectiveness (τ_e).

To calculate $C_{m_{i_t}}$, flight test data from Figures 23 through 29 was used to obtain values of δ_e for center of gravity locations at a constant C_L of 0.5 (this was the value used for the rigid analysis). In this manner a slope $\Delta X_{cg} / \Delta \delta_e$ was obtained from Figure 35.

From previous flight tests it was determined that the aircraft tail incidence was too high in that up elevator was necessary for almost all flight conditions (note Figure 2). Therefore, after all other flight tests were completed the tail incidence was lowered 5 degrees. The aircraft was then flown at C_L of 0.5 at three center of gravity locations and elevator position recorded. As $\Delta X_{cg} / \Delta \delta_e$ should not change with tail incidence a line was faired through these points with the $\Delta X_{cg} / \Delta \delta_e$ slope found previously.

From Reference 13:

$$C_{m_\delta} = C_L \frac{\Delta X_{cg}}{\Delta \delta_e}$$

(If $C_{L_{wing}} = C_{L_{\cancel{tail}}}$) A/C

and: $C_{m_\delta} = \tau_e \, C_{m_{i_t}}$

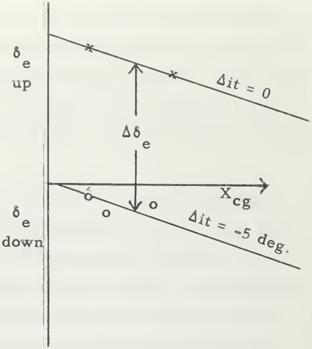

δ_e
up
$\Delta \delta_e$
$\Delta it = 0$
X_{cg}
δ_e
down
$\Delta it = -5$ deg.

Therefore:

$$1. \quad C_{m_{i_t}} = \frac{C_L}{\tau_e} \frac{\Delta X_{cg}}{\Delta \delta_e}$$

and:

$$\tau_e = \frac{\Delta \alpha_t}{\Delta \delta_e} = \frac{5 \text{ deg.}}{\Delta \delta_e}$$

From Figure 35 τ_e was found to be 0.55. Using this value of τ_e, the slopes $\Delta X_{cg} / \Delta \delta_e$ from Figure 35, and equation 1:

$$C_{m_{i_{t_{5.0}}}} = -1.0$$

$$C_{m_{i_{t_{7.0}}}} = -1.23$$

These values will be discussed in the results section of the report.

Other Aspects of Flight Test

Some of the other unique features of the aircraft effected flight test procedures. The semi-open cockpit induced a chill factor that had a decided effect on pilot response during the late winter months. Also, the open cockpit proved a problem for voice transmission. This was solved by wearing an oxygen mask with valves removed. This procedure cut the background noise to a very low level.

Due to the aft mounted propeller any loose gear in the cockpit could easily reach the propeller arc and be responsible for a fabric puncture. Thus, everything in the cockpit was of necessity tied down.

The low aerodynamic mass of the aircraft made it very susceptible to light gust, and to obtain usable data extremely smooth air was required. Figure ~~25~~ 33 shows a noise trace on a day that would normally be considered quite smooth.

Ground handling of the aircraft was reminiscent of sea plane operation and was a three man job. The ability of the aircraft to use sod runway greatly simplified the flight test, however.

In all respects the three pilots concerned were quite pleased to be able to obtain a small taste of open cockpit and the scream of wires that was so typical of early aviation.

DISCUSSION OF RESULTS

Definition of Problem

The original purpose of this investigation was to determine the applicability of standard analytical techniques on predicting static and dynamic stability of an inflatable airplane. It was assumed that the major factor influencing any deviation from rigid analysis for this aircraft would be fuselage bending. A secondary effect would be wing torsion and bending affecting lift curve slope (C_{L_α}) with changes with dynamic pressure (q). The change in C_{L_α} with q was obtained from Reference 4 which is a report on full scale wind tunnel test of the aircraft. As this data was available and accounts for flexibility effects on the wing and tail, it was decided to concentrate on the effects of fuselage bending.

The result of research was that there are many different opinions as to the effect of fuselage bending on such things as movement of stick fixed neutral and maneuver points (N_o and N_m). It was then determined that a further investigation of the effects of fuselage bending on longitudinal stability might be profitable. This aircraft would seem to be an ideal vehicle for this type of investigation in that fuselage stiffness could be varied by changing internal pressure.

All references agreed that fuselage bending was an overall destabilizing effect, and were in general agreement that N_m would move forward, except for Reference 9. Reference 9 stated that N_m would move aft due to a change in aircraft center of lift. The movement of N_o was not in agreement, however, in that there was difference of opinion in how far N_o should move forward relative to N_m.

It was anticipated that the change in N_m and N_o between internal pressures of 5 psig and 7 psig would answer some of these questions.

It was considered that a valid measure of fuselage bending would be changes in $C_{m_{i_t}}$, and it was expected that $C_{m_{i_t}}$ would be reduced by fuselage flexibility.

Predicted Results

The rigid analysis was made using classical techniques of References 2 and 7. An effort was made to determine tail efficiency (η_t) by a wake survey mentioned in the preflight test. This yielded a value of η_t of 1.3 that resulted in a $C_{m_{i_t}}$ for the rigid aircraft of -1.397. A full scale wind tunnel value of C_{L_α} was chosen at the test q of 8.46 psf.

The results of this analysis were a predicted N_o of 47.5 percent MAC, N_m of 59.9 percent MAC, phugoid period of 15.7 seconds, and a damping ratio of 0.245.

For the semi-rigid analysis $C_{m_{i_t}}$ and C_{L_α} were factored out of the equations of motion and a root locus plotted showing effects of changing $C_{m_{i_t}}$ and C_{L_α} (Figures 16 and 17). The excursion of C_{L_α} was expected to be from 3.0 to 5.0 and values of 3.0, 4.0, and 5.0 per radian were used for the root locus plot.

A static bending test of the fuselage was made at internal pressures of 5.0 psig and 7.0 psig. (This procedure may be found in the flight test procedures section of the report.) The results of this test yielded predicted values of $C_{m_{i_t}}$ of -1.08 at 7 psig and -0.87 at 5.0 psig.

Flight Test Results

Although the flight test determination of $C_{m_{i_t}}$ and τ_e were done at the end of the program a flight test value of τ_e ~~is~~ was necessary to correlate other flight test results with predictions. From Figure 35, τ_e was found to be 0.55. (The method used may be found in the flight test section of the report.) This value of τ_e compared favorably with the predicted value of 0.6 and is considered valid.

From the flight test for stick fixed static stability, $N_{o_{5.0}}$ was found to be 40.0% MAC and $N_{o_{7.0}}$ 42.0% MAC. Due to the scatter in data this result can only be considered as a qualitative indication in the movement of N_o with fuselage bending. A possible explanation for the scatter in the neutral point data may be due to a change in position of the elevator potentiometer string tie down point. As velocity is changed, the leading edge of the horizontal stabilizer may deform and twist, consequently displacing the tie down point. Since the neutral point tests were made over a speed range of 45 to 65 knots, the tie down point would not remain in the same relative position, thereby making the elevator readings differ from the exact value in an unpredictable manner. It can be concluded that N_o moves forward with fuselage bending; however, the use of this data to conclude the relative movement of N_o and N_m with flexibility is questionable.

Although the slope of the δ_e / C_L versus X_{cg} curve is not considered valid in finding $C_{m_{i_t}}$, for a non-rigid aircraft, values of $C_{m_{i_t}}$ were calculated from Figure 30. $C_{m_{i_t\ 5.0}}$ was found to be -1.33 and $C_{m_{i_t\ 7.0}}$ -1.54, using the flight test value of τ_e. Using the data of the δ_e / C_L curves, Figures 23 through 29, as plotted on Figure 35, $C_{m_{i_t\ 5.0}}$ was found to be -1.0 and $C_{m_{i_t\ 7.0}}$ -1.23. This procedure is described in the flight test section of the report and is considered a much more valid method of determining $C_{m_{i_t}}$ for a non-rigid aircraft than using the slope of the δ_e / C_L versus X_{cg} curve. These values are in excellent agreement with those predicted by the static bending test.

The flight test results for N_m were found to have much less scatter and are considered to be of significance. $N_{m\,5.0}$ was found to be 46.0% MAC and $N_{m\,7.0}$ 49.2% MAC. These results show a definite destabilizing trend with bending. The slopes of the δ_e / n

versus X_{cg} curves of Figure 31 yielded values of $C_{mi_{t\,5.0}}$ of -1.07 and $C_{mi_{t\,7.0}}$ of -1.40. These values are in good agreement with magnitudes predicted by the static bending test.

Phugoid periods and damping ratios obtained from rigid analysis and flight test data were plotted on the root locus diagram, Figure 17. The results of these tests showed a definite trend towards instability with increasing fuselage flexibility. $C_{mi_{t\,5.0}}$ was found to be -0.8 and $C_{mi_{t\,7.0}}$ -1.25 by the mean position of the plots of flight test periods and damping ratios at the two inflation pressures.

The short period mode of dynamic motion could not be investigated with the instrumentation installed. It's high damping ratio of 0.89 and low time constant of 0.2 seconds precluded its usefulness for these tests. The reason for the high damping ratio is the very low aerodynamic mass of this aircraft.

Table III is a comparison of C_{mi_t} values found from static bending tests and four flight test methods. This comparison shows close agreement by all methods and a definite destabilizing trend with fuselage bending.

The results of flight test thus verified the values of C_{mi_t} and τ_e used in the rigid analysis. It can then be stated with some certainty that the rigid analysis was valid. This being the case, N_o moved forward from the rigid value to the 5 psig value 7.5% MAC while N_m moved forward 13.9% MAC. While the movement of N_o between 5 psig and 7 psig is not well defined, its movement from a rigid value to a flexible value is considered to be of such validity as to warrant mention.

It may therefore be stated that for this aircraft N_m and N_o are both destabilized by fuselage flexibility and it is further indicated that N_m moves further forward than N_o.

The high frequency aircraft oscillation mentioned in the flight test procedures was determined to be caused by elevator flutter. This

flutter was found to become excited at 63 knots IAS with 5 psig internal airframe pressure.

A movie supplement to Reference 4 relates a similar motion occurring at 7 psig pressure at a dynamic pressure of 20 psf in the full scale wind tunnel. The motion was felt to be excited by elevator flutter in that fixing the elevator to the horizontal stabilizer stopped the motion.

Figure 22 shows a recording of the motion during flight test at 5 psig internal pressure. From the recording it was found that the elevator oscillation was from amplitudes of + 2 degrees to + 13 degrees at a frequency of 5 cps. It is felt that this is the same motion described in the wind tunnel test.

In the wind tunnel analysis the cause of the flutter was attributed to control looseness. This assumption is felt to be valid in that the elevator can be moved approximately 5 degrees with the stick fixed at 7 psig internal pressure. At a lower pressure the elevator is, of course, more loose. It is felt that, this being the case, the elevator flutter could occur at a dynamic pressure of 12 psf (63 knots IAS), and that the motion observed in flight test is the same motion previously seen in the wind tunnel.

CONCLUSIONS

It is concluded that rigid analysis techniques will predict longitudinal stick fixed dynamic stability of the YAO-3G inflatable airplane to a good degree of accuracy. Static stability predictions are not as accurate but do indicate typical values. The aircraft when operated at recommended internal pressures is of sufficient rigidity as not to deviate far from rigid analysis. However, if rigid values of $C_{m_{i_t}}$ are corrected by factors obtained from static bending tests, accurate predictions may be obtained for both dynamic and static stick fixed stability.

The effect of fuselage flexibility of this aircraft was destabilizing to both dynamic and static stability. The phugoid mode was rendered less stable by increased flexibility. Both stick fixed neutral and maneuver points moved forward; however, it was indicated that N_m is destabilized to a larger extent than N_o.

REFERENCES

1. Societe de Fabrication D'Instruments de Mesure, Flight Recorder Technical Information Manual, Publication No. TD 175, 12 August 1954.

2. Seckel, E.: Stability and Control of Airplanes and Helicopters, Academic Press, New York, 1964.

3. Goodyear Aircraft Corporation, Summary Aerodynamic Report of One-Man Inflatoplane, GER 9942, 10 August 1960.

4. McLemore, H. C.: Wind Tunnel Investigation of the Aerodynamic and Structural-Deflection Characteristics of an Inflatable Airplane, NASA TMX-680, August 1962.

5. Gilruth, R. R.: Analysis and Prediction of Longitudinal Stability of Airplanes, NACA TR 711.

6. Lyons, D. J. and Bisgood, P. L.: An Analysis of the Lift Slope of Airfoils of Small Aspect Ratio, including Fins, with Design Charts for Airfoils and Control Surfaces, R and M No. 2308, January 1945.

7. Perkins, C. D. and Hage, R. E.: Airplane Performance, Stability and Control, John Wiley and Sons, Inc., New York, 1950.

8. Babister, A. W.: Aircraft Stability and Control, Pergamon Press, New York, 1961.

9. Klawans, B. B. and Johnson, H. I.: Some Effects of Fuselage Flexibility on Longitudinal Stability and Control, NACA TN 3543, April 1956.

10. Collar, A. R. and Grinsted, F.: The Effects of Structural Flexibility of Tailplane, Elevator, and Fuselage on Longitudinal Control and Stability, R and M No. 2010, September 1942.

11. Lyon, H. M. and Ripley, J.: A General Survey of the Effects of Flexibility of the Fuselage, Tail Unit, and Control Systems on Longitudinal Stability and Control, R and M No. 2415, July 1945.

REFERENCES (Continued)

12. Fingado, H. and Taylor, A. S.: An Approximate Method of Estimating the Effect of Elastic Deformability of the Aircraft Structure on the Maneuver Point, R and M No. 3019, March 1950.

13. Perkins, C. D.: Methods for Obtaining Aerodynamic Data Through Steady State Flight Testing, April 1950.

14. Higgins, G. J.: Unpublished class notes presented at the U.S. Naval Postgraduate School, Monterey, California.

TABLE I

Aircraft Specifications

General:	
Span	23.2 ft
Length	22.0 ft
Height	7.2 ft
Wing area	124.3 ft^2
Wing loading	4.42 #/ft^2
Thrust loading	1.69 #/ft^2
Moment of Inertia (Iy)	277.2 slug ft^2
Weights:	
Weight empty	315 lbs
Useful load - 1 pilot	194 lbs
Fuel	10 gal 61 lbs
Gross take-off	570 lbs
Engine:	
Available sea level static thrust	220 lbs
at combat rating	at 3750 RPM
Propeller diameter	47 in
Height of thrust line above CG	3.14 ft
Minimum fuel consumption at sea level cruise	20.2 #/hr

TABLE I (Continued)

Wing:	
Airfoil section	NACA 0015
Area (S)	124.3 ft^2
Span (b)	23.2 ft
Aspect ratio (AR)	4.44
Taper ratio (λ)	1
Chord ($\bar{c}$)	5.31 ft
Ailerons:	
Chord $c_a / \bar{c}$	20.4 %
Area S_a ~~/S~~	6.41 ft^2
Horizontal Tail:	
Area (S_t)	21.05 ft^2
Span (b_t)	6.66 ft
Chord ($\bar{c}_e$)	3.167 ft
Tail volume ($V_t = \frac{S_t}{S} \frac{\ell_t}{\bar{c}}$)	.399
Elevators:	
Chord (c_e)	1.33 ft
Area	8.86 ft^2
Elevator travel	30 up to 25 down
Vertical Tail:	
Area (S_v)	15.31 ft^2
Span (b_v)	3.92 ft
Chord (c_v)	4.416 ft
Rudder:	
Mean chord	1.66 ft
Area	5.0 ft^2

TABLE II

Analog Computer Potentiometer Values

Pot	Quantity	Value	Pot Setting
1	δ_e	.1	.1
2	$K \frac{\ell_e}{V_o}$	5.954	.5954
3	$K \tau_e$	24.18	.2418
4	$K(1 - \frac{d\varepsilon}{d\alpha})$	23.38	.2338
5	$K(\frac{\ell_t}{V_o} \frac{d\varepsilon}{d\alpha})$	2.502	.2502
6	$C_{m_{i_{t/2}}}$	$C_{m_{i_{t/2}}}$	$C_{m_{i_{t/2}}}$
7	$V_o M_V$	.681	.681
8	$K\, C_{m_{\alpha_{f/2}}}$	.3625	.3625
9	$\frac{K}{2} \bar{x}_a a_w$	$.806\ C_{L_\alpha}$	$.0806\ C_{L_\alpha}$
10	$D_V - T_V$	.236	.236
11	$\frac{g}{V_o}$	.3815	.3815
12	$\frac{g}{V_o}$	.3815	.3815
13	$\frac{2g}{e \pi AR} a_w$	$.0736\ C_{L_\alpha}$	$.0736\ C_{L_\alpha}$
14	V_o	84.45	.8445
15	$\frac{g}{C_L V_o} a_w$	$.781\ C_{L_\alpha}$	$.0781\ C_{L_\alpha}$
16	L_V	.761	.761
17	V_o	84.45	.8445
18	V_o	84.45	.8445

Note: $K = \frac{2g}{C_L\, c\, (\frac{ky}{\bar{c}})^2} = 40.3$

Voltage-quantity ratios

$\Delta\alpha, \Delta\theta, \Delta\delta_e$: 1 v. = .01 rad

$\Delta\dot{\alpha}, \Delta\dot{\theta}$: 1 v. = .01 rad/sec

Δu, Δv: 1 v. = 1 ft/sec

Δh: 1 v. = 1 ft

TABLE III

$C_{m_{i_t}}$ Values

	Rigid	7.0 psi	5.0 psi
Rigid Analysis using Classical Techniques	-1.397	-	-
Static Bending Test (with factors applied to rigid values)	-	-1.08	- .87
Static Flight Tests a) gradient of $\frac{d\delta_e}{dn} = \frac{C_{L_{n=1}}}{\tau_e C_{m_{i_t}}}$ $\tau_{e_{exp}} = .55 \quad C_{L_{n=1}} = .5$ Figure 31	-	-1.4	-1.07
b) gradient of $\frac{d\delta_e}{dC_L} = \frac{1}{\tau_e C_{m_{i_t}}}$ Figure 30	-	-1.54	-1.33
c) $C_{m_{i_t}} = \frac{C_L}{\tau_e} \frac{\Delta\delta_e}{\Delta x_{cg}}$ Figure 35	-	-1.23	-1.0
Dynamic Flight Tests Figure 17	-	-1.25	- .8
Average	-	-1.30	-1.01

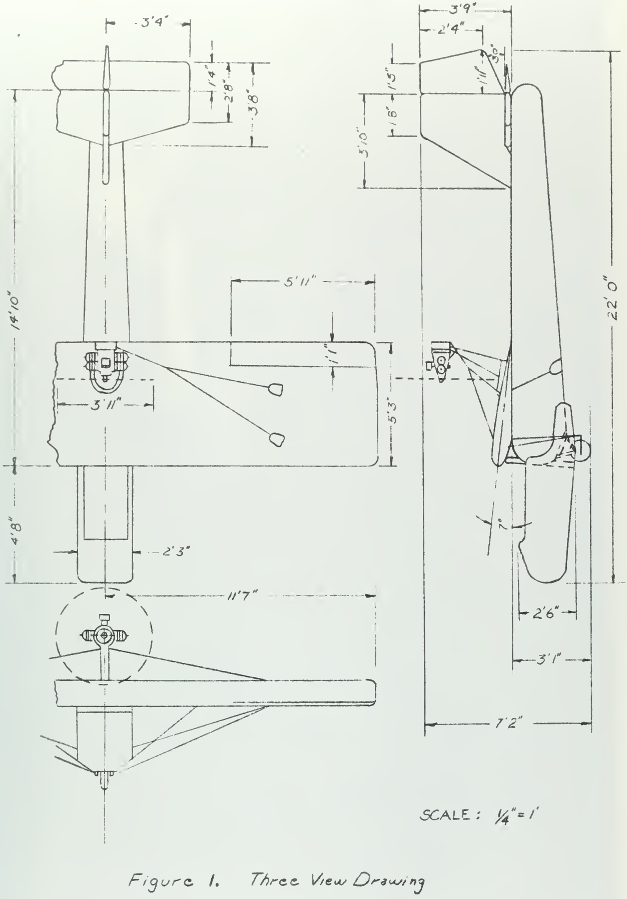
3'4"
1'4"
2'8"
3'8"
14'10"
5'11"
1'1"
5'3"
3'11"
4'8"
2'3"
11'7"
3'9"
2'4"
30°
1'5"
1'11"
1'6"
3'10"
22'0"
7°
2'6"
3'1"
7'2"

SCALE: 1/4" = 1'

Figure 1. Three View Drawing

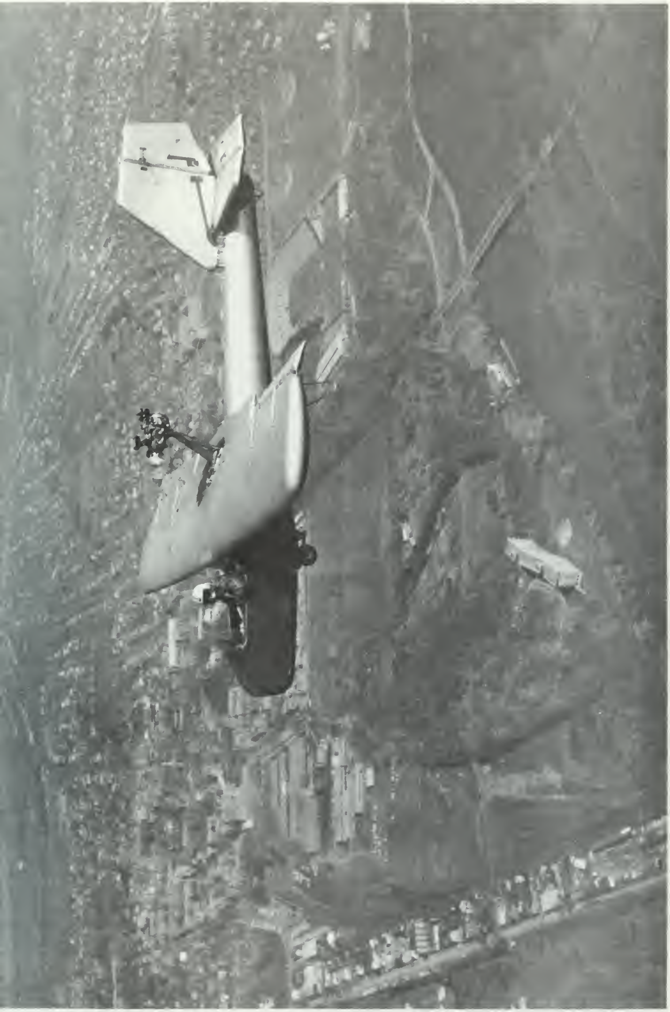

Figure 2. Air Photo of Aircraft.

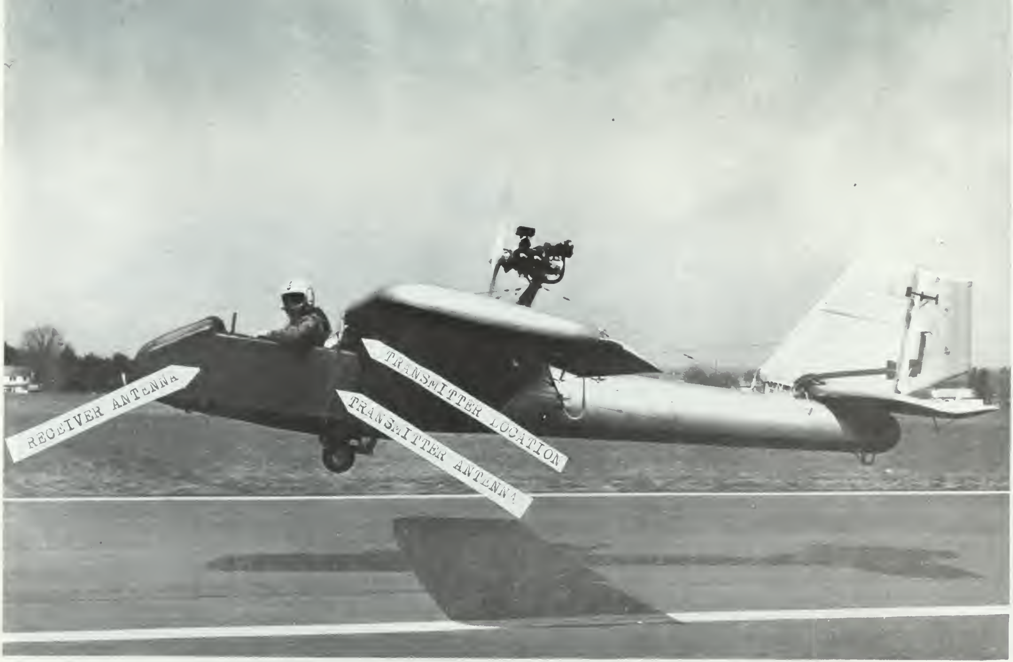
RECEIVER ANTENNA
TRANSMITTER LOCATION
TRANSMITTER ANTENNA

Figure 3. Left Side View of Aircraft.

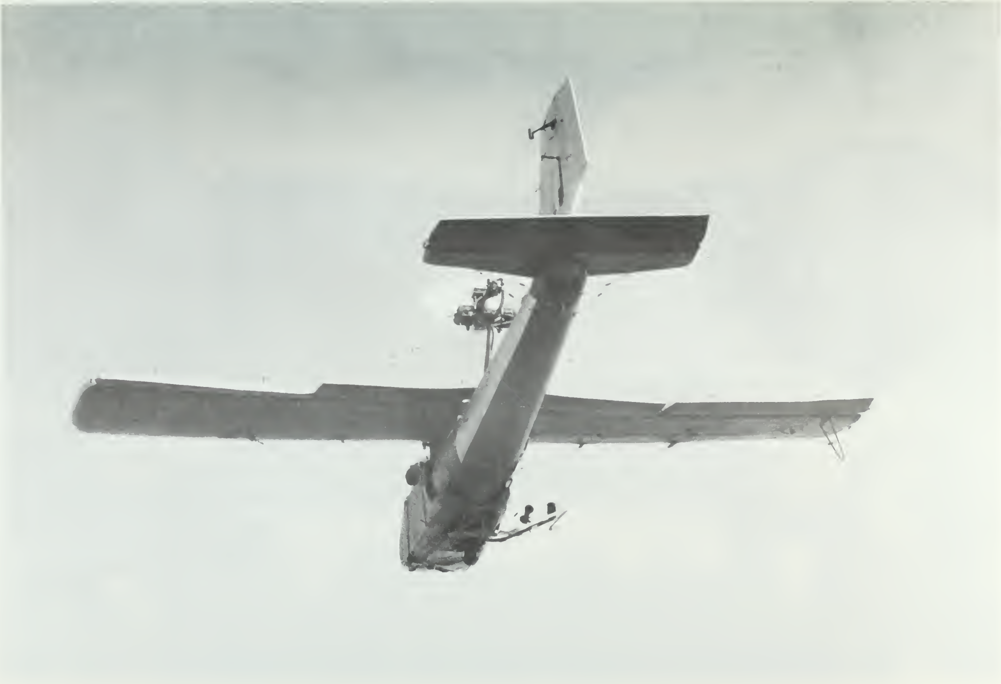

Figure 5. Rear View of Aircraft.

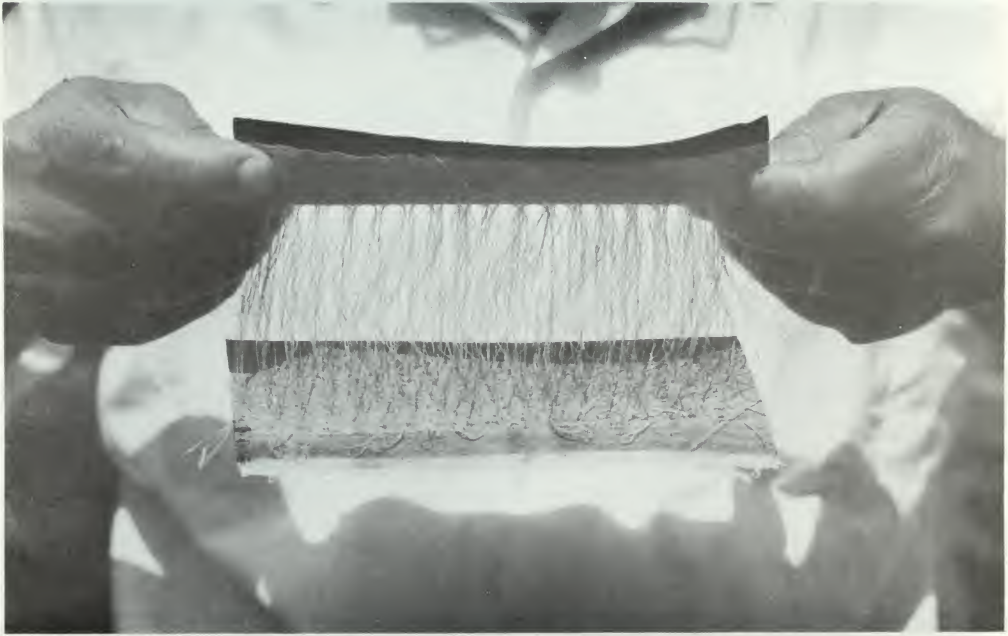

Figure 6. Exposed View of Air Mat.

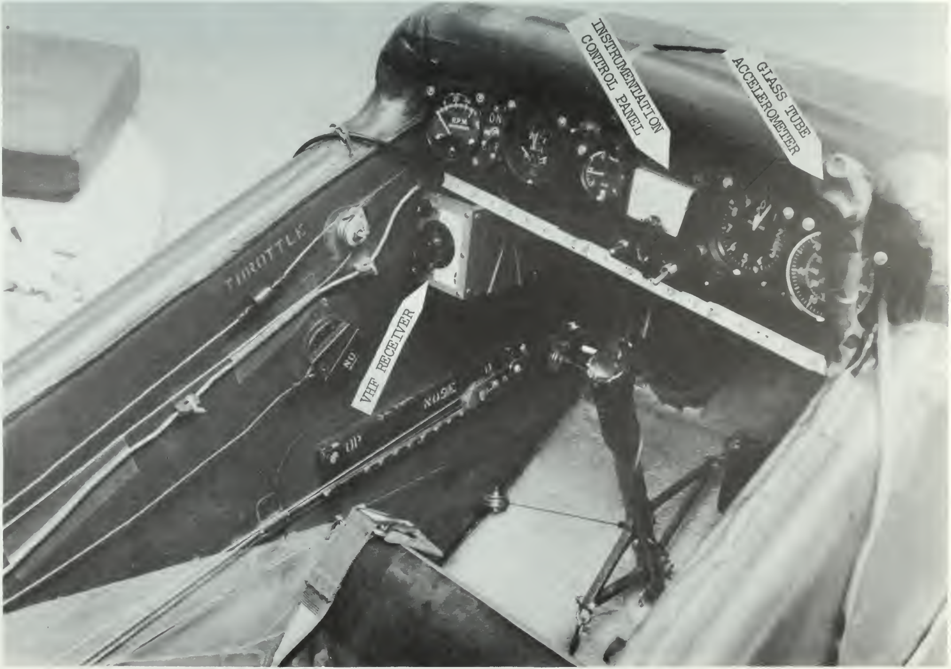
INSTRUMENTATION CONTROL PANEL
GLASS TUBE ACCELEROMETER
R.P.M.
ON
THROTTLE
VHF RECEIVER
NOSE
UP
ON

Figure 7. Instrument Panel.

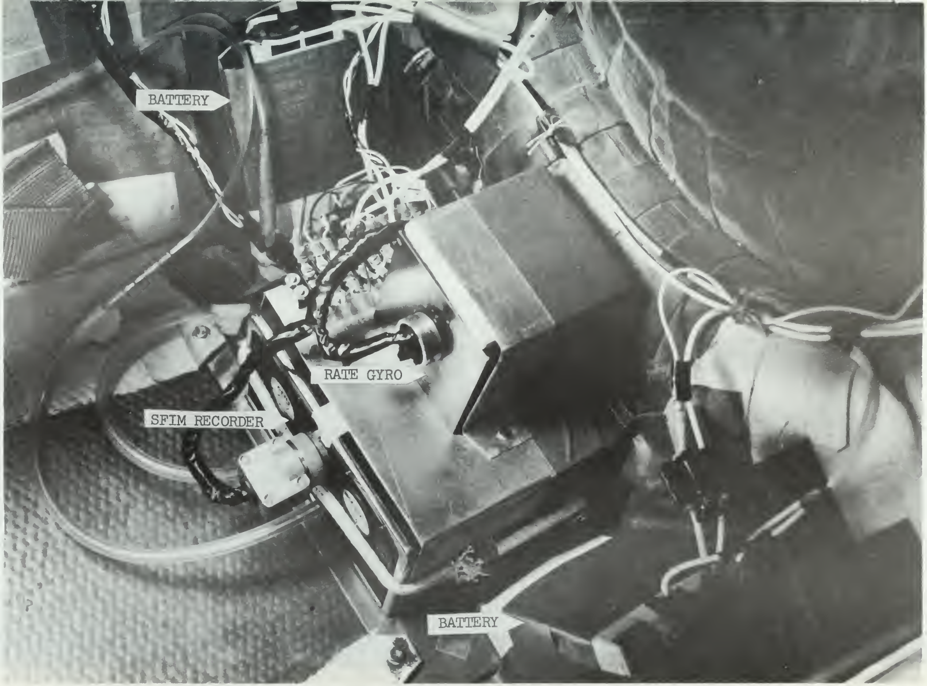
BATTERY
RATE GYRO
SFIM RECORDER
BATTERY

Figure 8. Recorder and Battery Location; Rear of Cockpit.

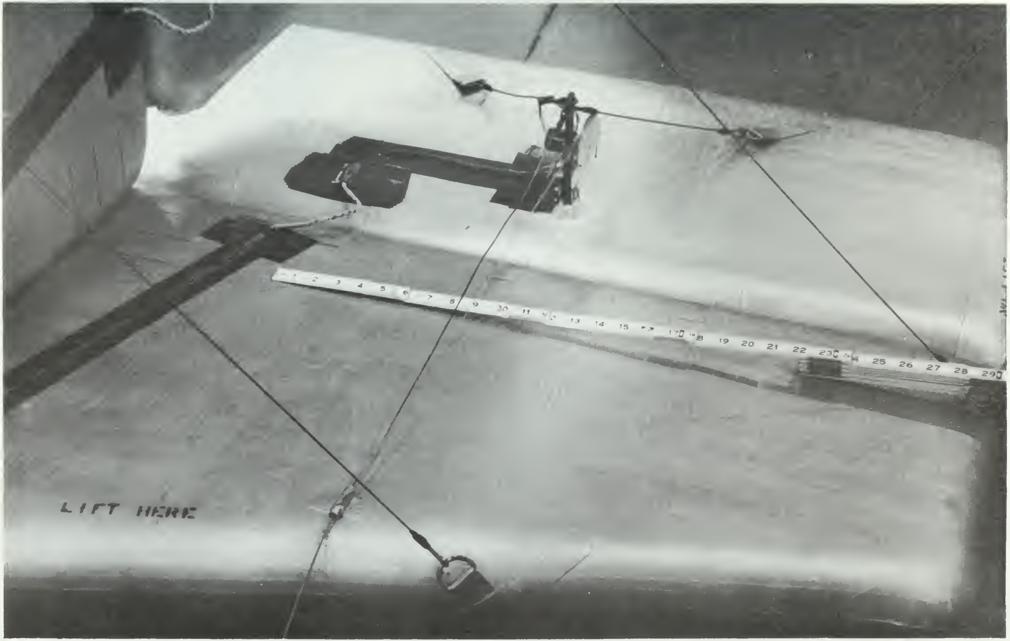

Figure 9. Elevator Potentiometer Location.

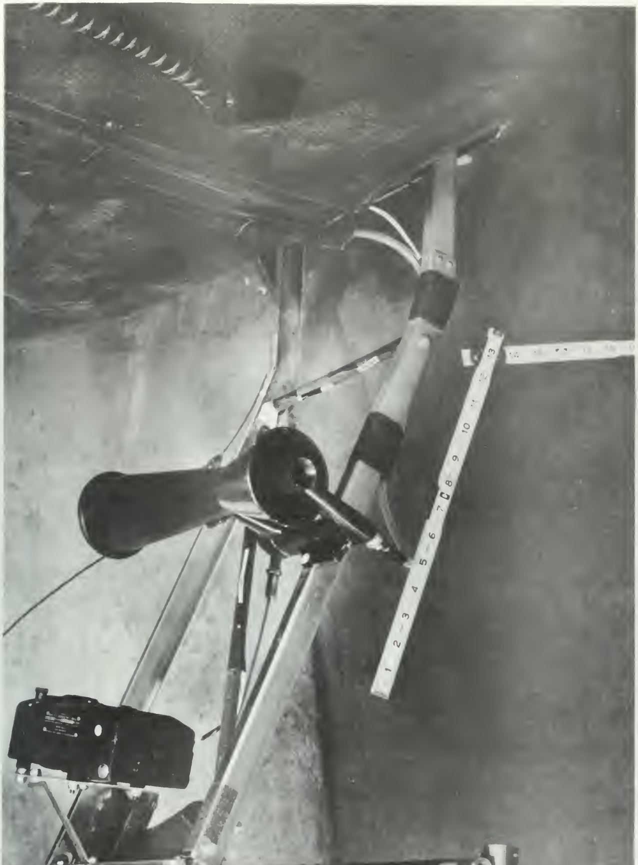

Figure 10. Angle of Attack Boom, Camera and Venturi.

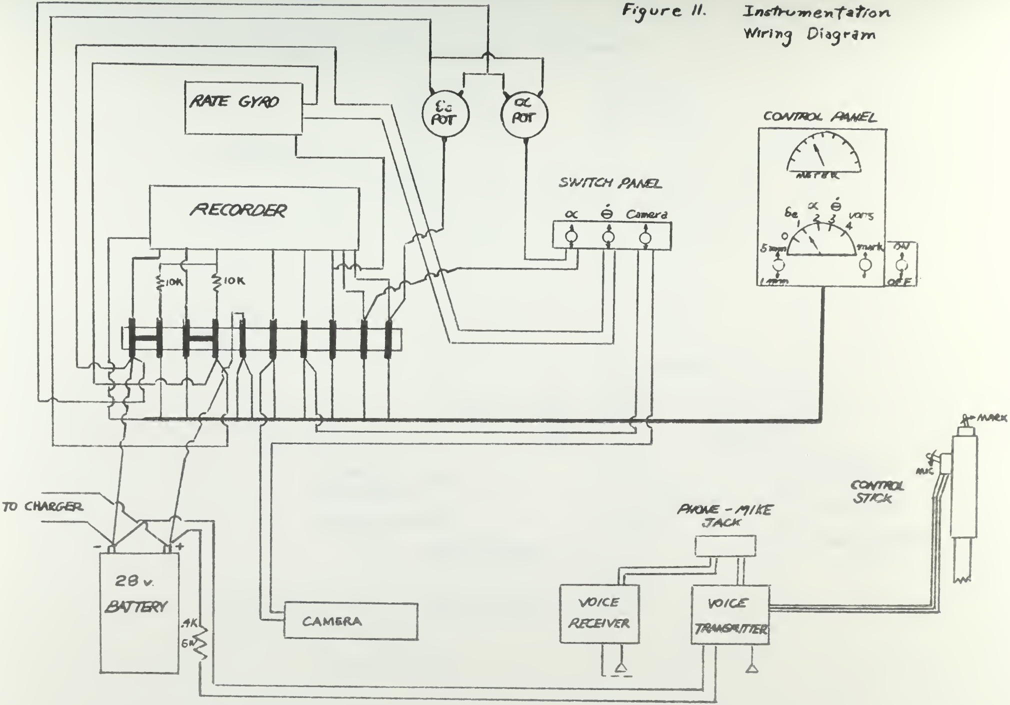

Figure 11. Instrumentation Wiring Diagram

RATE GYRO
δ_c POT
α POT
RECORDER
10K
10K
SWITCH PANEL
α
$\dot{\theta}$
Camera
CONTROL PANEL
METER
δ_e
α
$\dot{\theta}$
VOLTS
0
1
2
3
4
5 mm
1 mm
mark
ON
OFF
MARK
MIC
CONTROL STICK
TO CHARGER
-
+
28 v.
BATTERY
.4K
6W
CAMERA
PHONE - MIKE JACK
VOICE RECEIVER
VOICE TRANSMITTER

Figure 12. Instrumentation Schematic

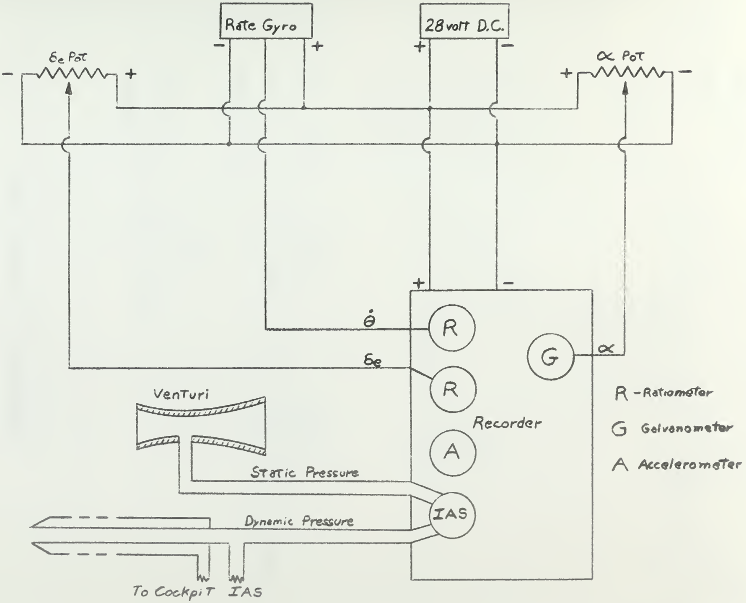
Rate Gyro
28 volt D.C.
δ_e Pot
α Pot
+
-
$\dot{\theta}$
δ_e
α
R
R
G
A
IAS
Recorder
R - Ratiometer
G Gelvanometer
A Accelerometer
VenTuri
Static Pressure
Dynamic Pressure
To Cockpit IAS

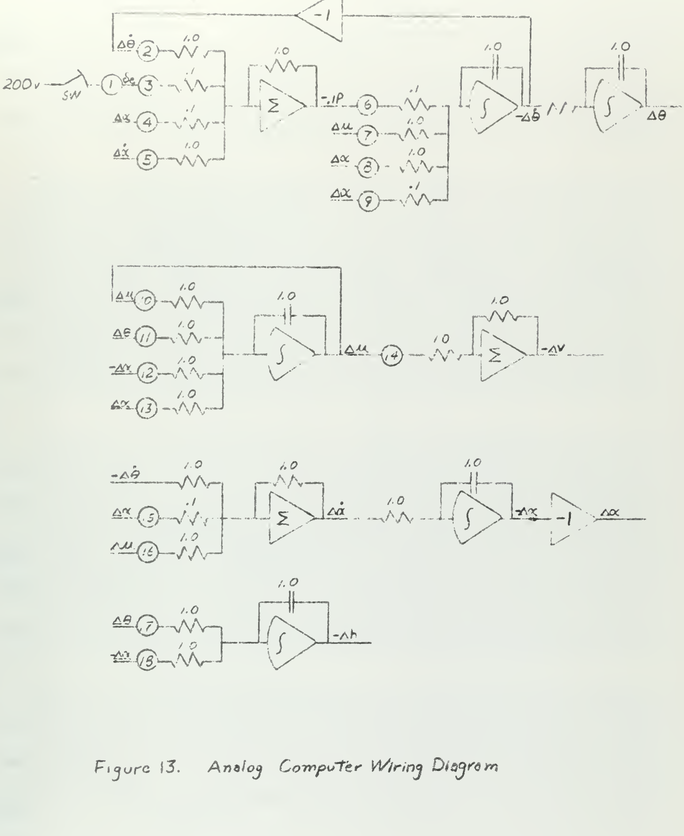
-1
1.0
200v
SW
1
δ_e
2
3
4
5
$\Delta\dot{\theta}$
$\Delta\alpha$
$\Delta\dot{\alpha}$
.1
Σ
-.1P
6
7
8
9
Δu
$\Delta\alpha$
$\Delta\dot{\alpha}$
∫
$-\Delta\dot{\theta}$
$\Delta\theta$
10
11
12
13
14
Δu
$\Delta\theta$
$-\Delta\alpha$
$\Delta\alpha$
$-\Delta V$
$-\Delta\dot{\theta}$
15
16
$\Delta\dot{\alpha}$
$-\Delta\alpha$
$\Delta\alpha$
17
18
$-\Delta h$

Figure 13. Analog Computer Wiring Diagram

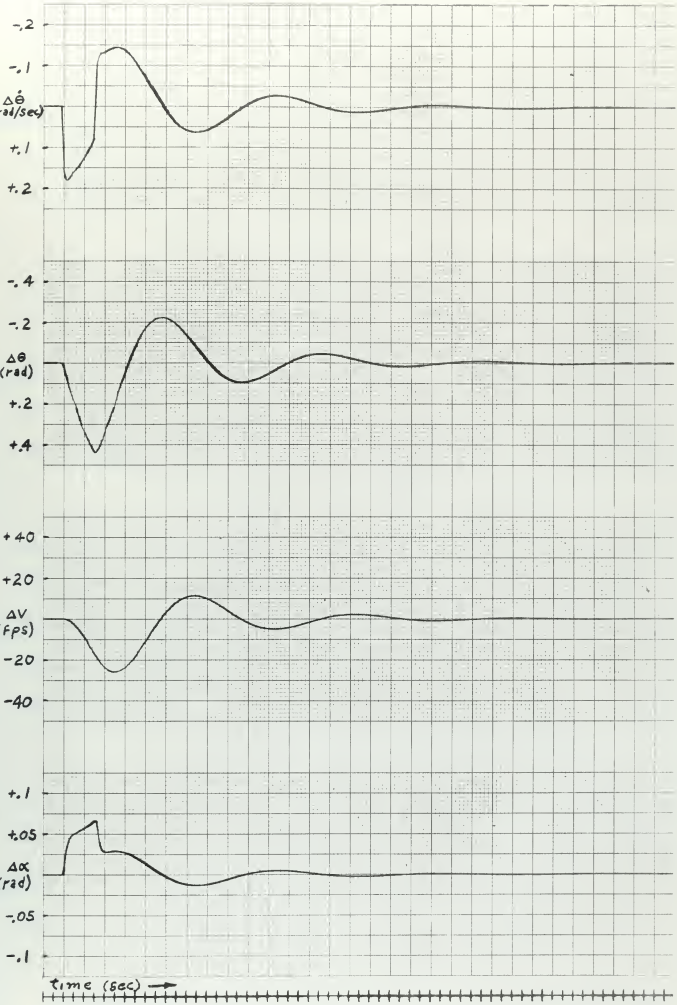

Figure 14. Analog Computer Solution. $C_{L_\alpha} = 4.18$, $C_{m_{i_T}} = 1.397$

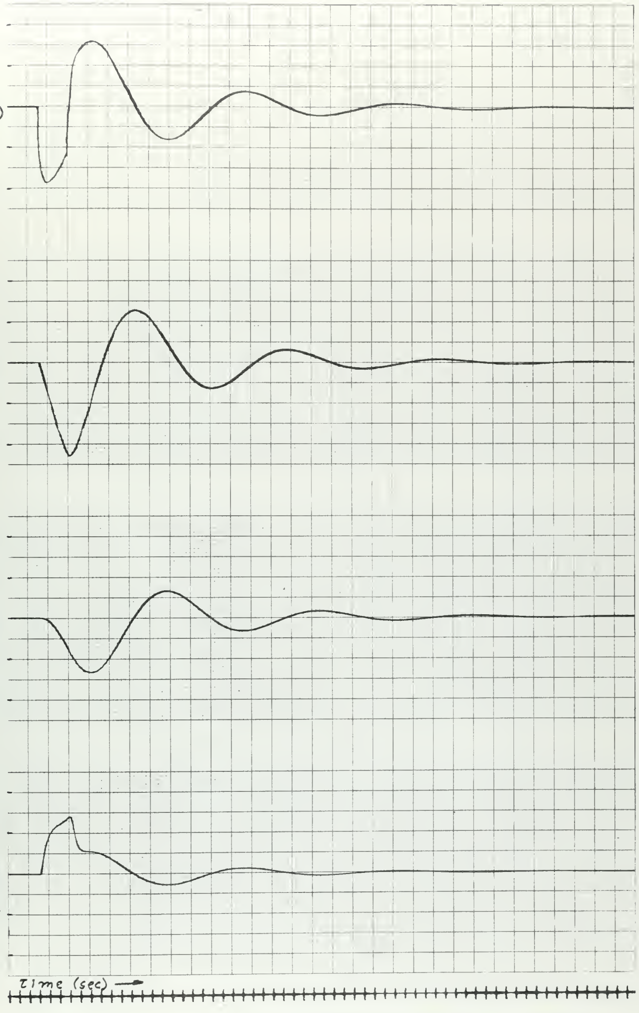

Figure 15a. Analog Computer Solution. $C_{L_\alpha} = 4.18$, $C_{m_{i_t}} = .8$

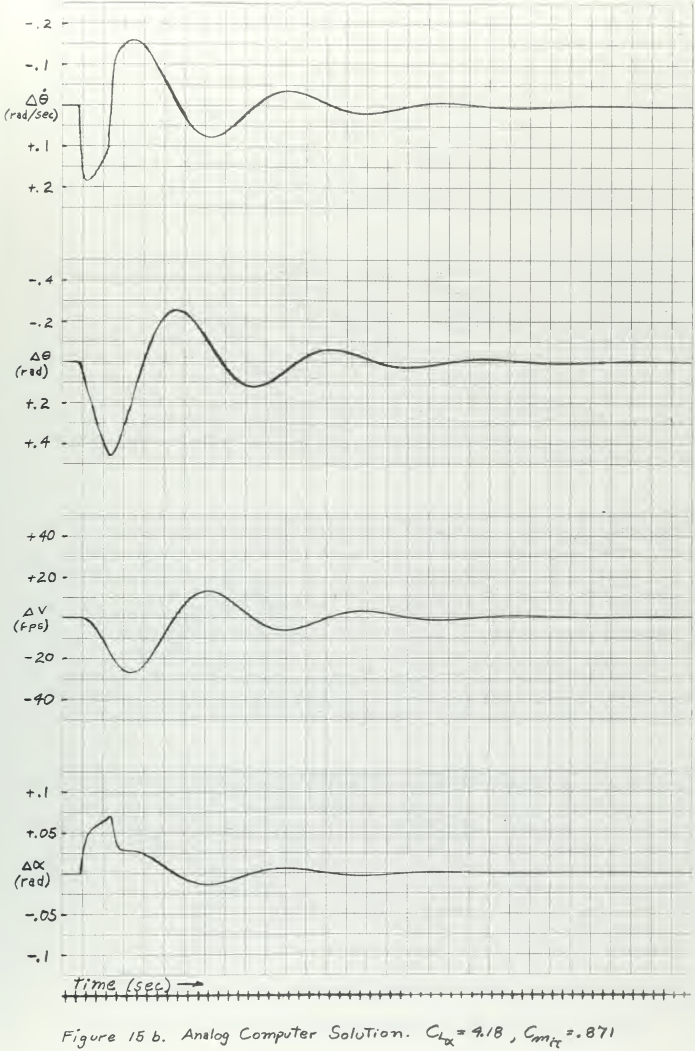

Figure 15 b. Analog Computer Solution. $C_{L_\alpha} = 4.18$, $C_{m_{\dot\alpha}} = .871$

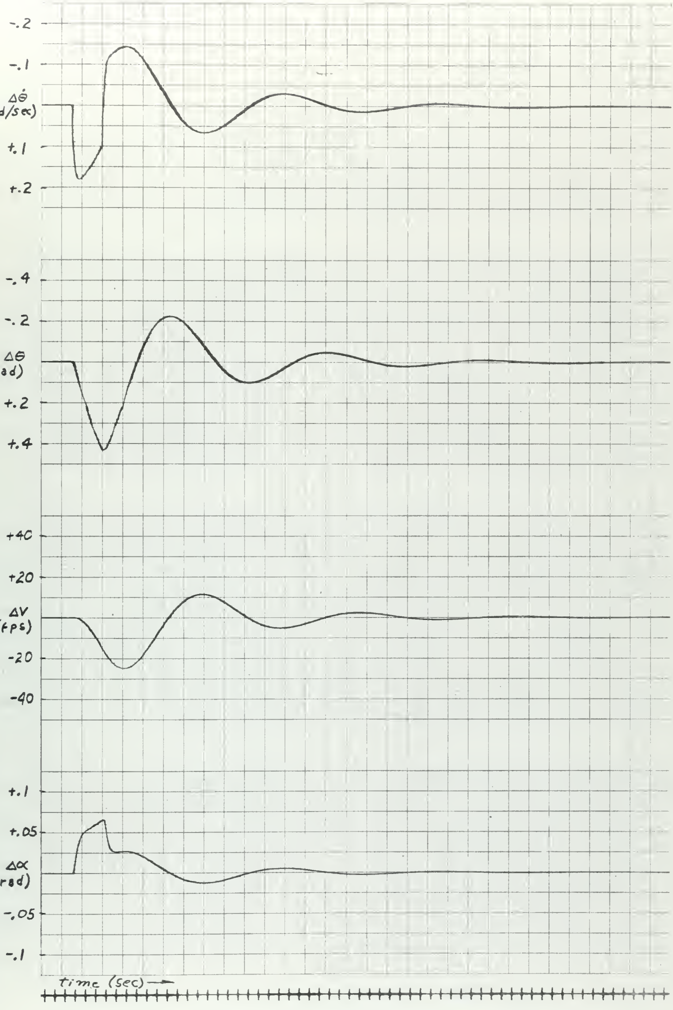

Figure 15c. Analog Computer Solution. $C_{L_\alpha} = 4.18$, $C_{m_{i_T}} = 1.075$

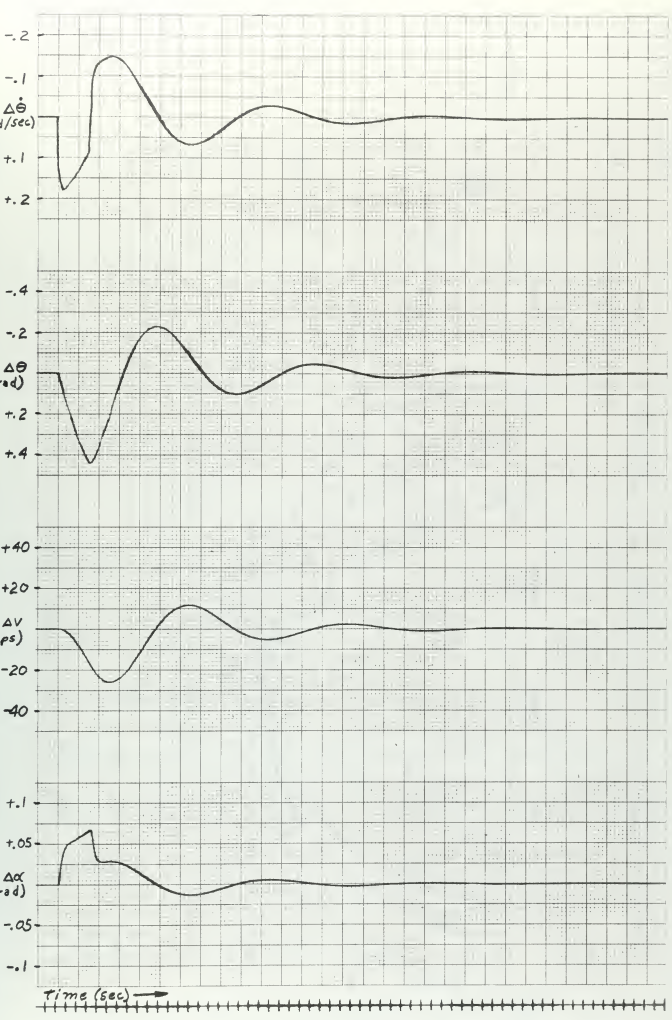

Figure 15d. Analog Computer Solution. $C_{L_\alpha} = 4.18$, $C_{m_{lc}} = 1.2$

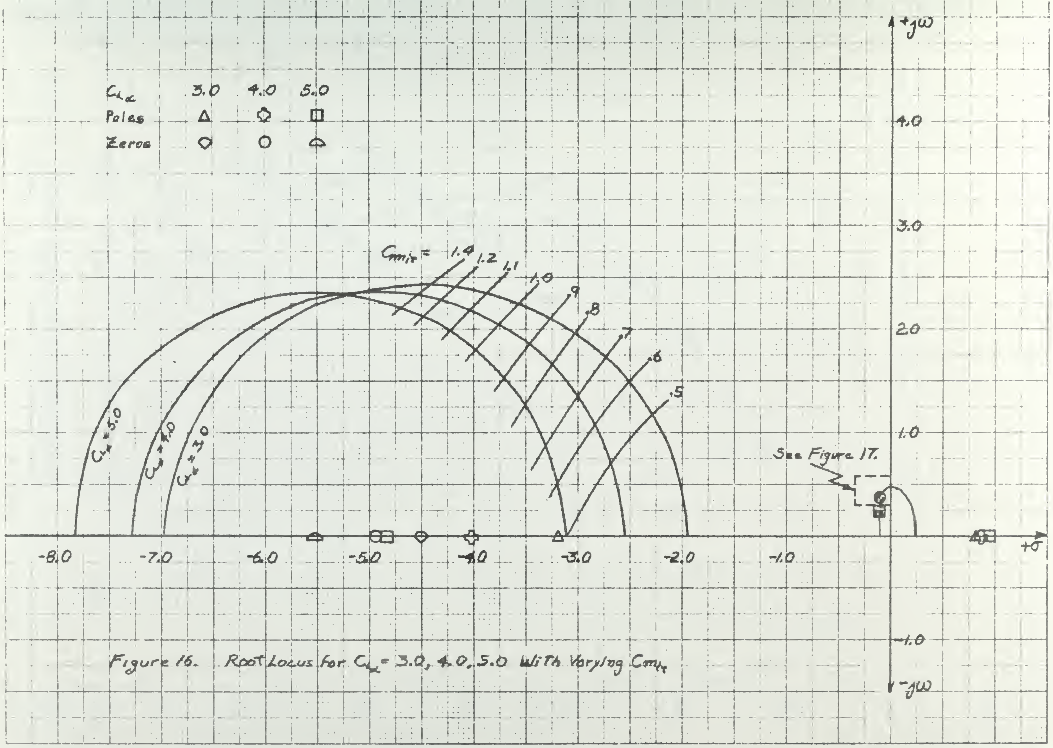

Figure 16. Root Locus for $C_{L\alpha}$ = 3.0, 4.0, 5.0 With Varying C_{m_q}

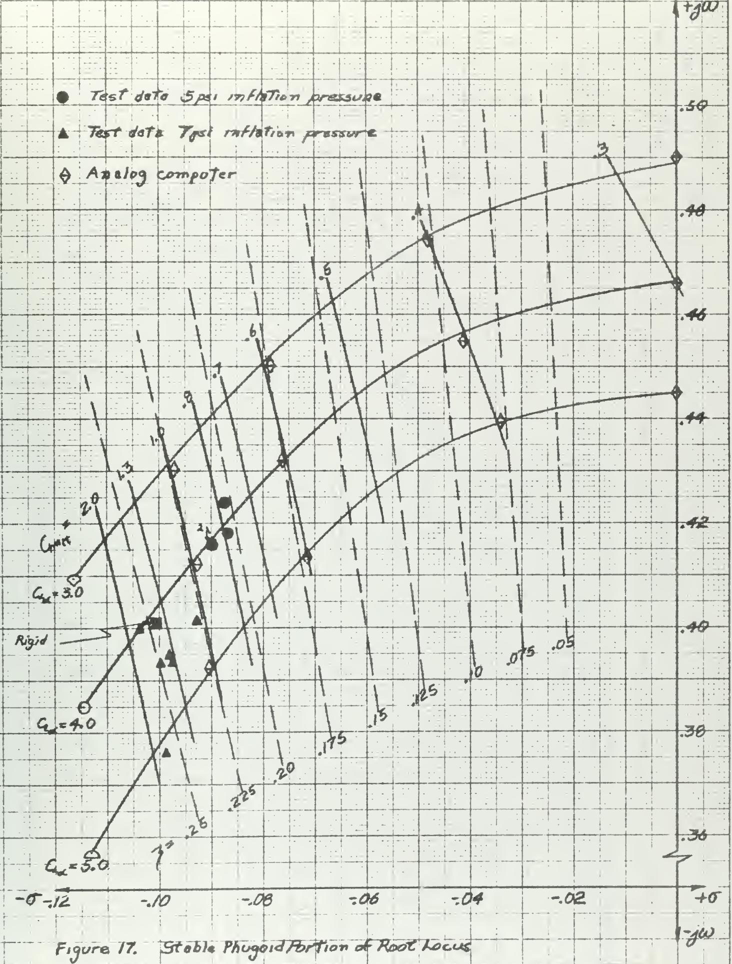

Figure 17. Stable Phugoid Portion of Root Locus

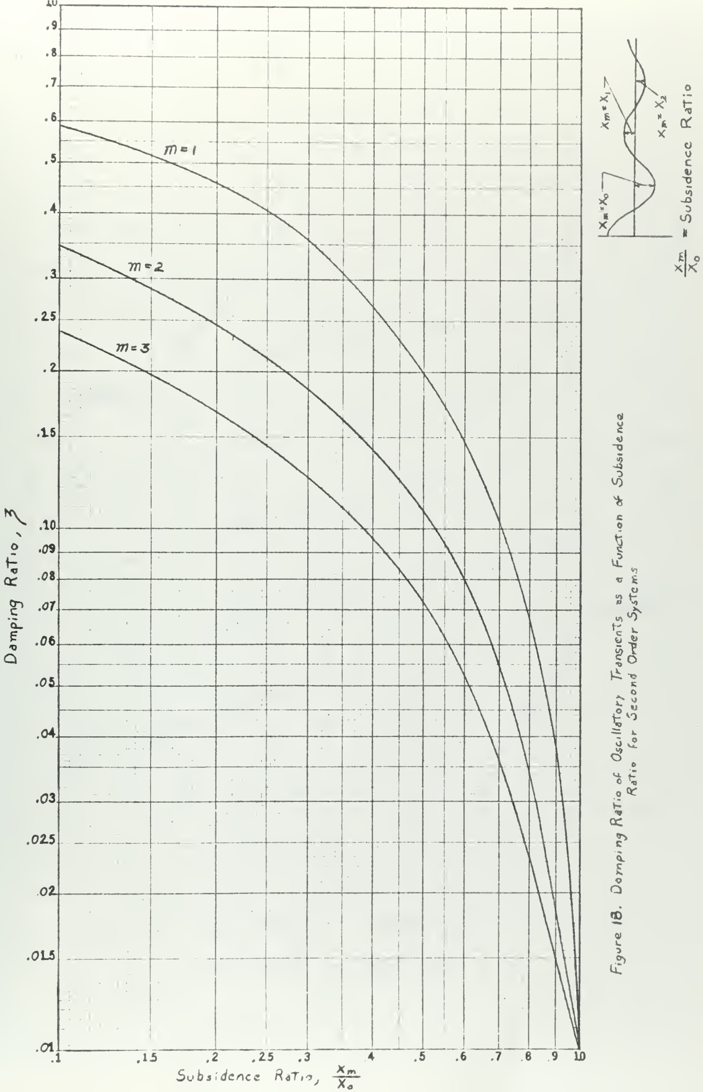

Figure 18. Damping Ratio of Oscillatory Transients as a Function of Subsidence Ratio for Second Order Systems

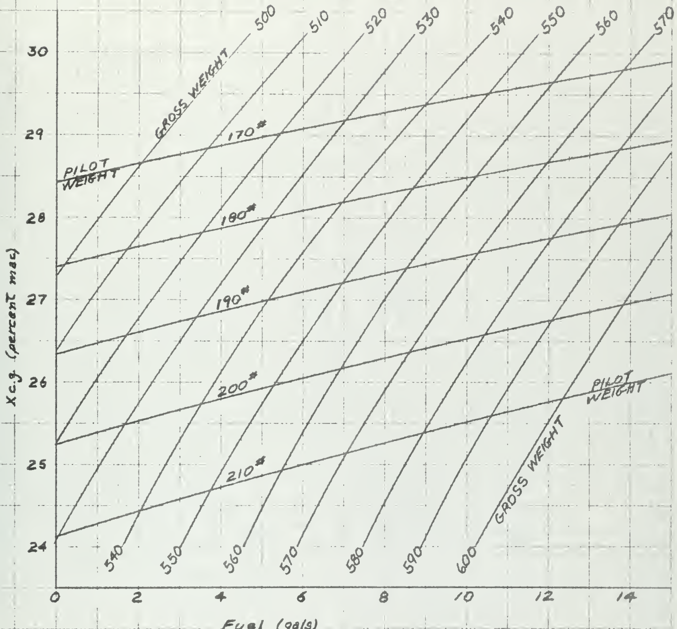

Figure 19. Center of Gravity and Gross Weight vs. Fuel Quantity and Pilot Weight

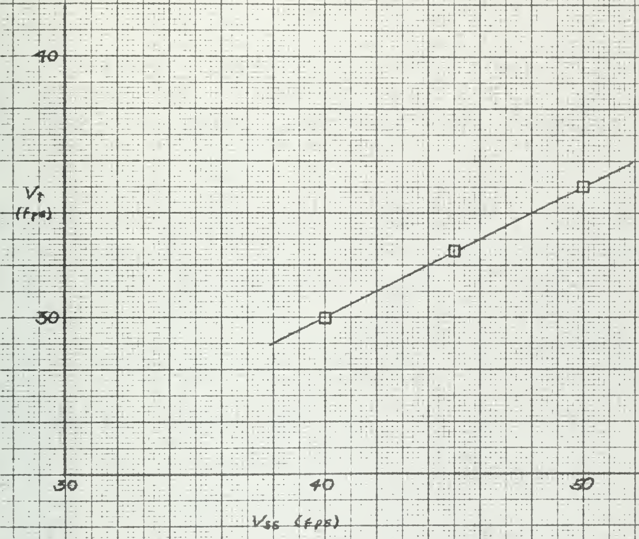

Figure 20. Wake Survey For Determination of η_r

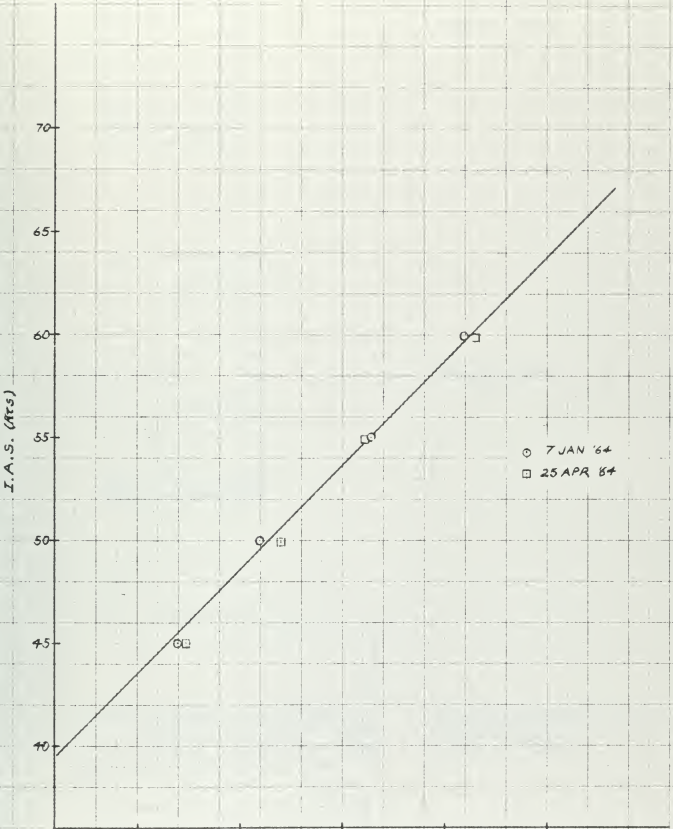

Figure 21. Airspeed Calibration

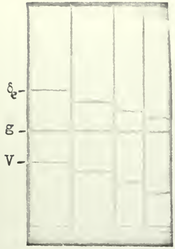

Neutral Point

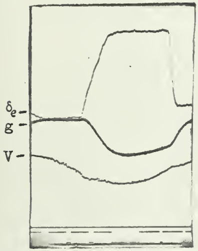

Maneuver Point

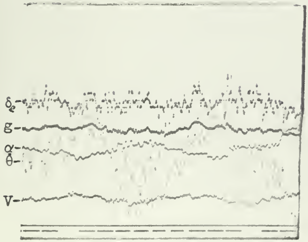

Aircraft Vibration Due To Elevator Flutter.

Figure 22. SFIM Recorder Tapes

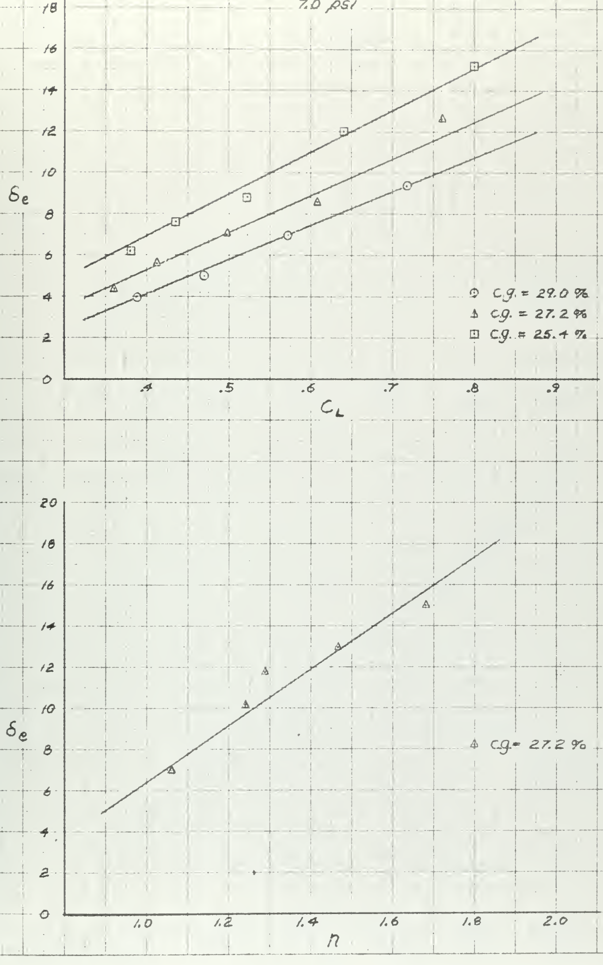

Figure 23. Flight Test Data

4-5-64

7.0 psi

Figure 24. Flight Test Data

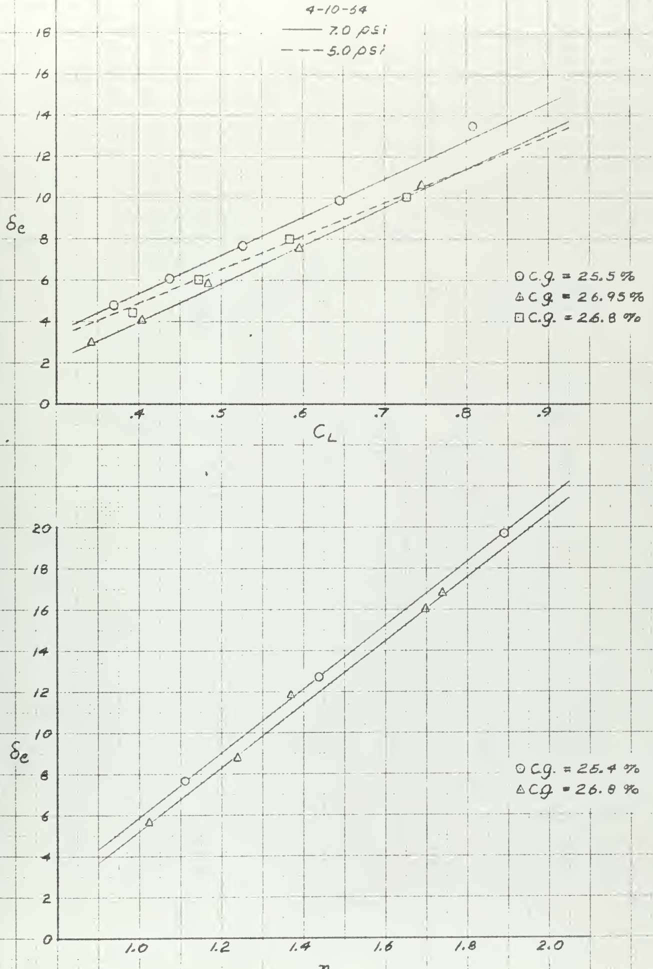

Figure 25. Flight Test Data

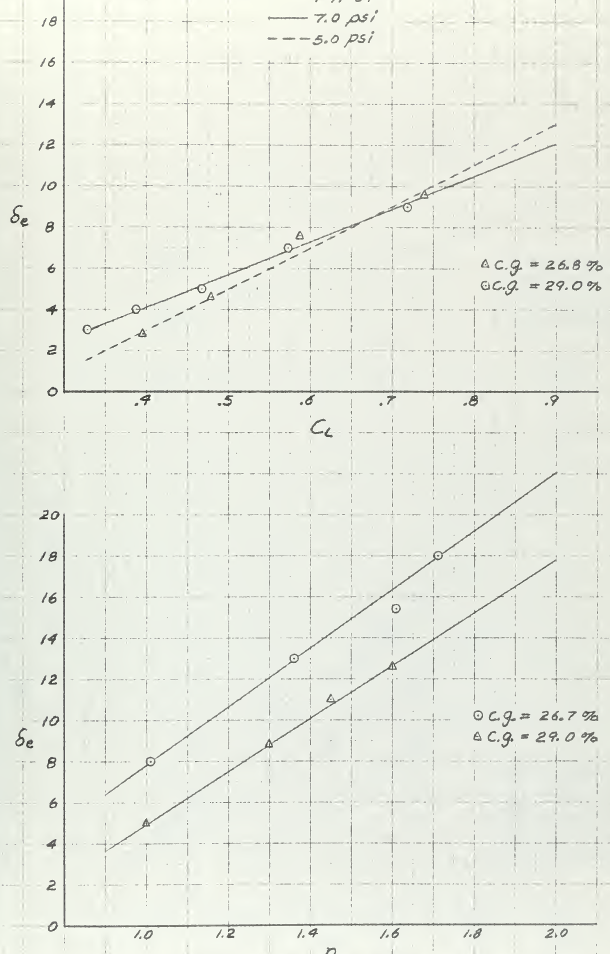

Figure 26. Flight Test Data

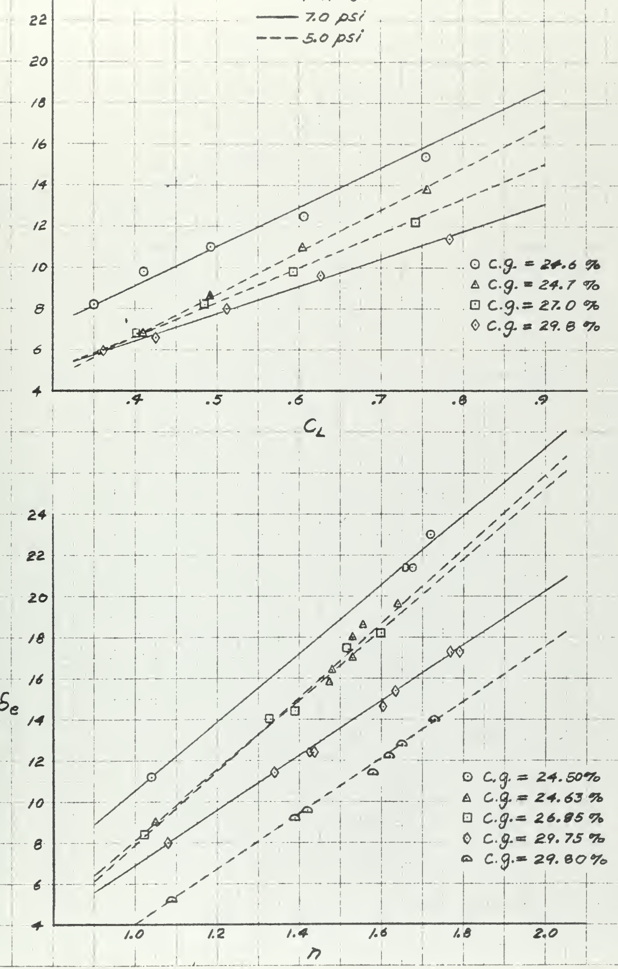

Figure 27. Flight Test Data

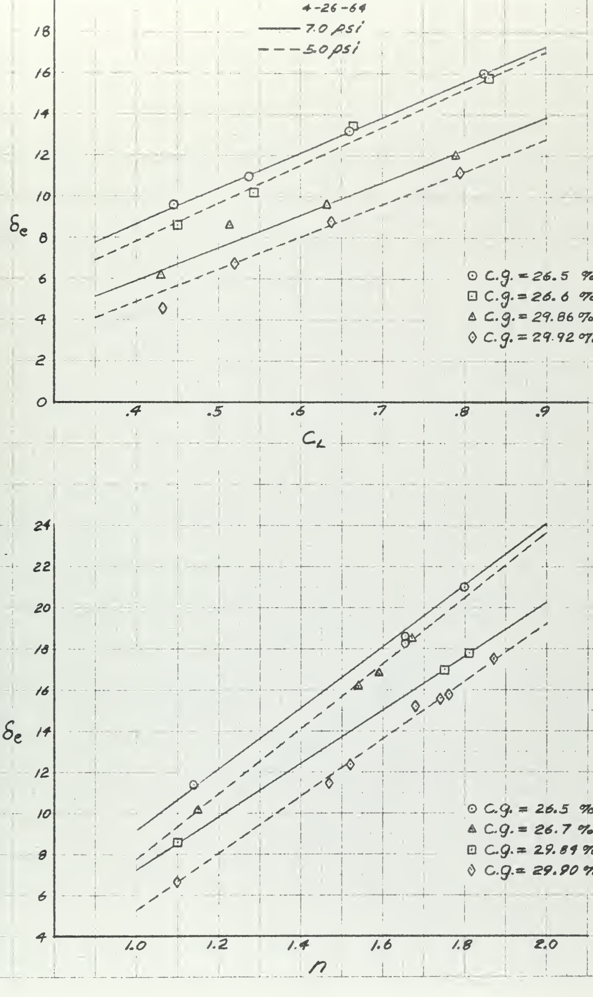

Figure 28. Flight Test Data

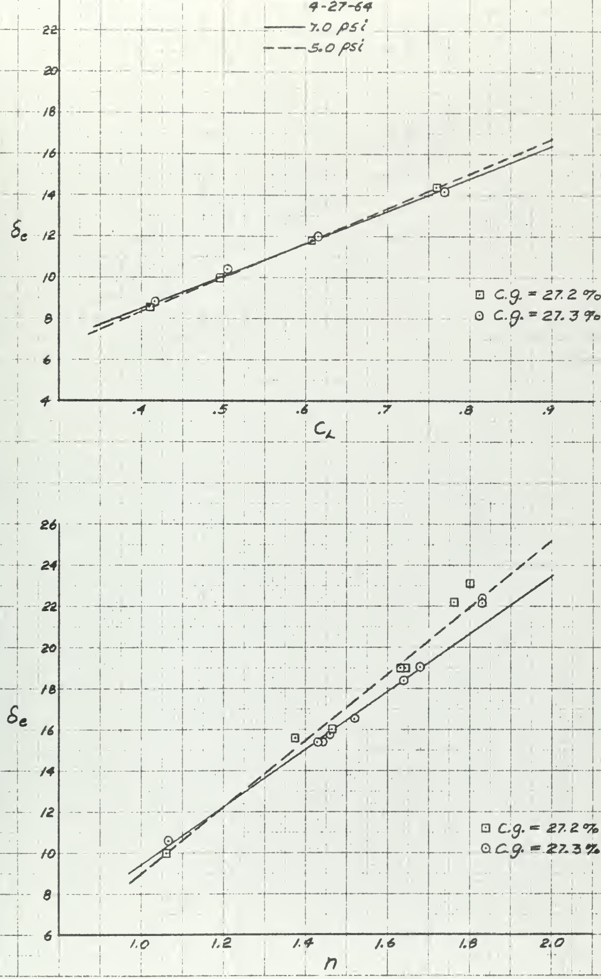

Figure 29. Flight Test Data

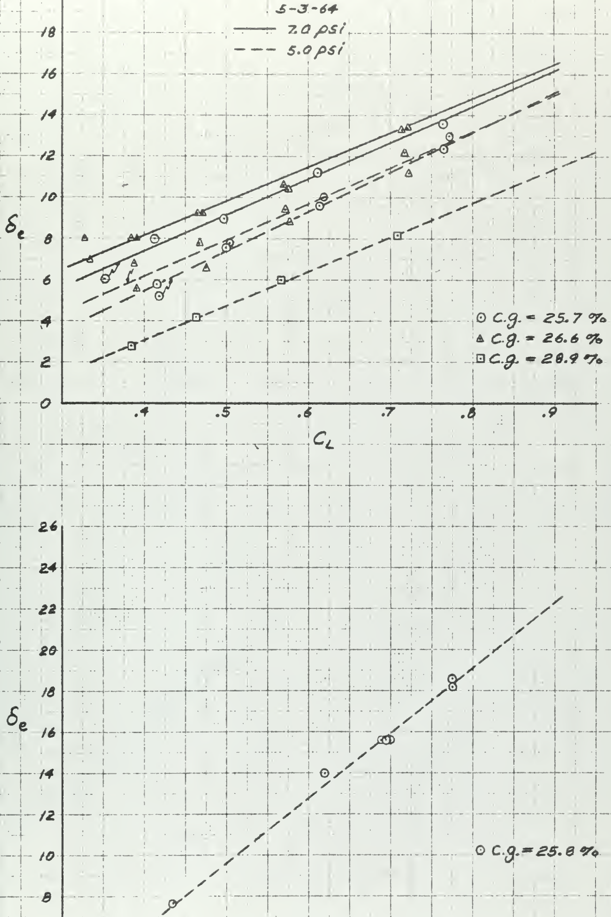

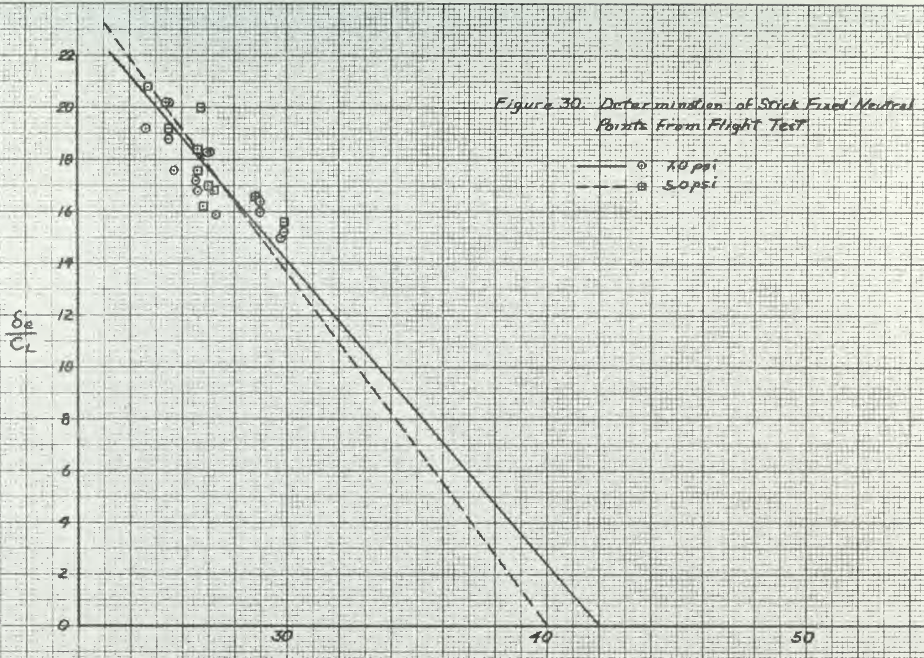

Figure 30: Determination of Stick Fixed Neutral Points From Flight Test

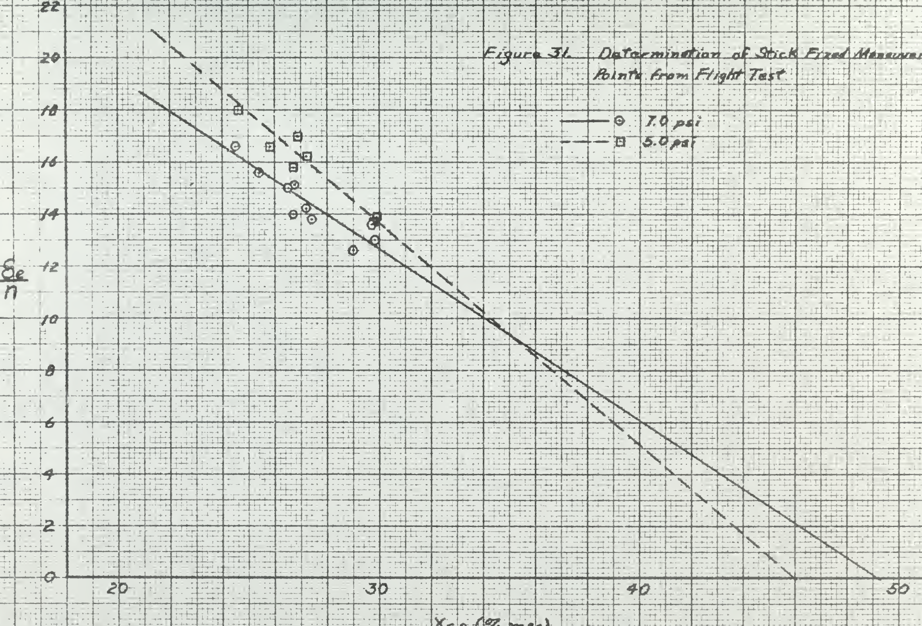

Figure 31. Determination of Stick Fixed Maneuver Points from Flight Test

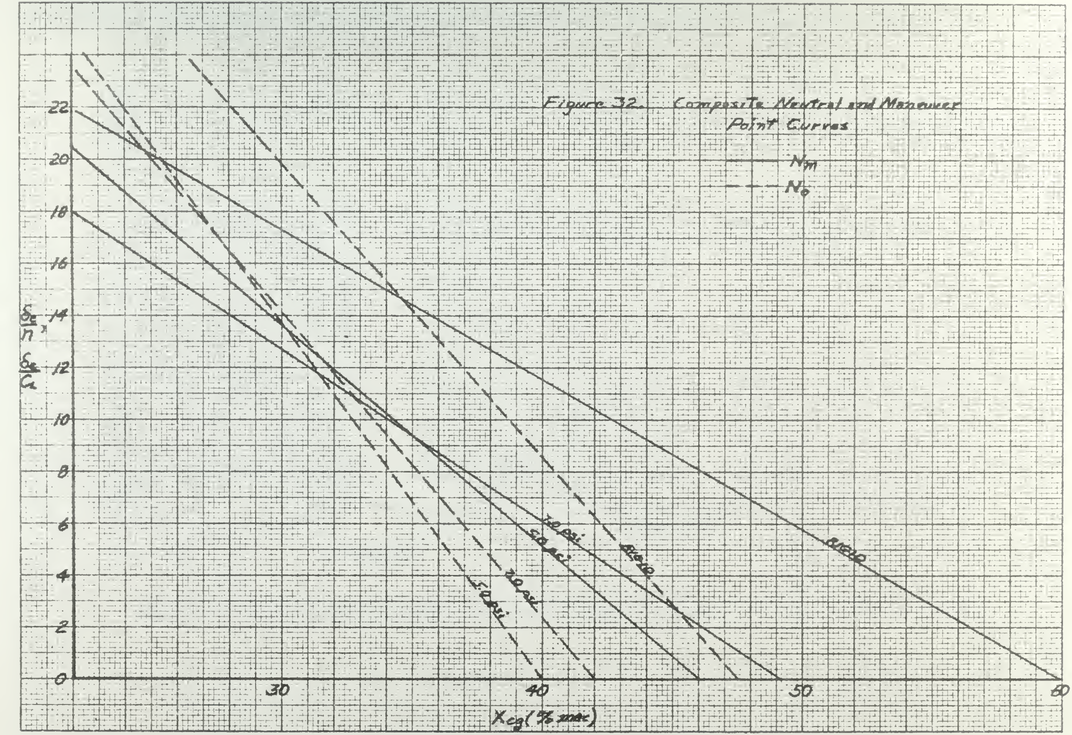

Figure 32. Composite Neutral and Maneuver Point Curves

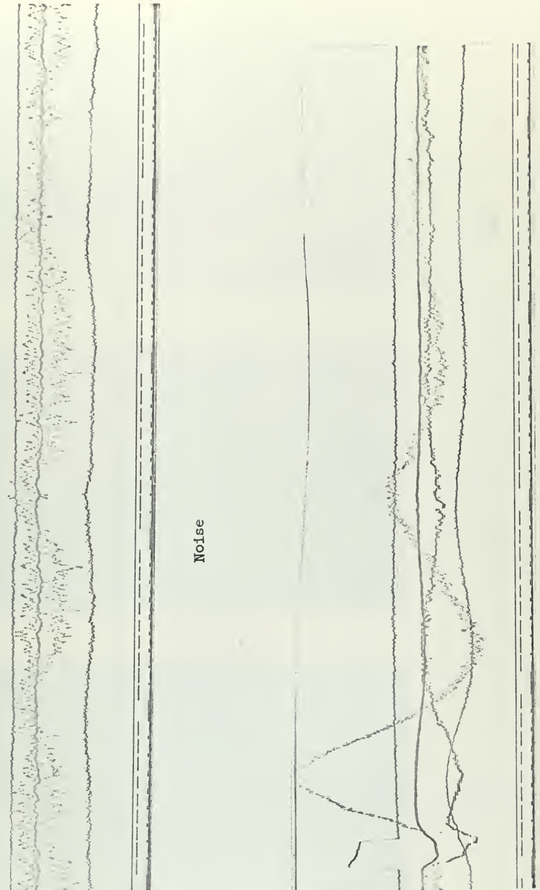

Noise

Phugoid

Figure 33. SFIM Recorder Tapes

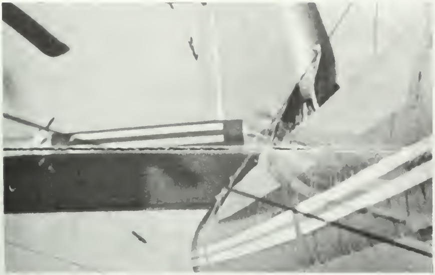

Level Flight Condition

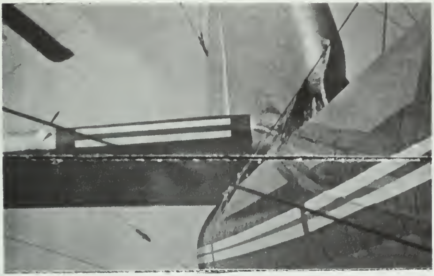

Deflection Due To
Up Load

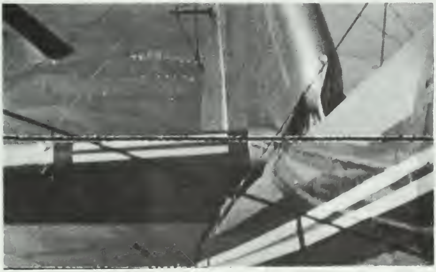

Deflection Due To
Down Load

Fig. 34. Selected Prints From Movie Camera Showing Fuselage Bending.

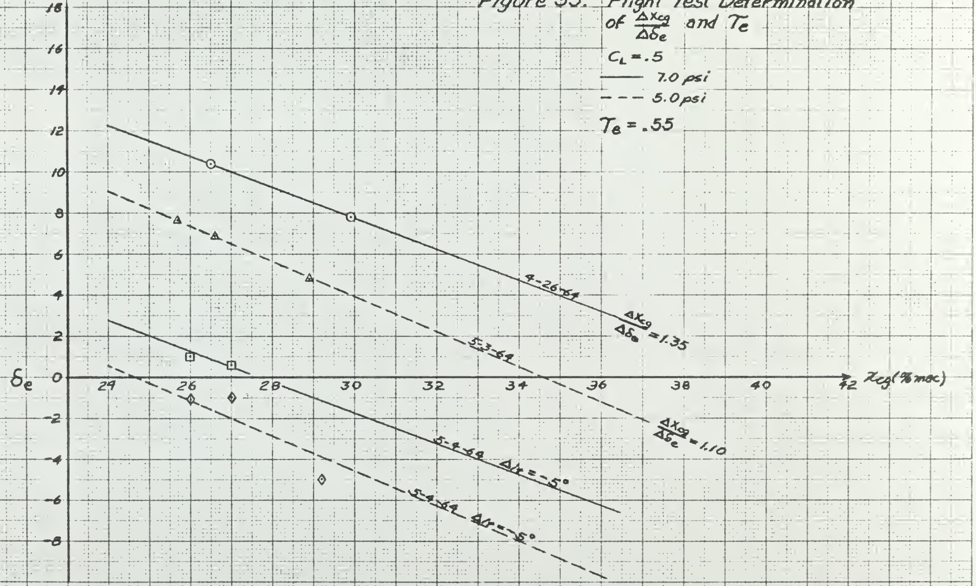
Figure 35. Flight Test Determination of $\frac{\Delta x_{cg}}{\Delta \delta_e}$ and τ_e

thesB458
Longitudinal stability of the Goodyear I
3 2768 002 13777 0
DUDLEY KNOX LIBRARY